Published in final edited form as:
Nat Neurosci. 2017 September ; 20(9): 1225–1235. doi:10.1038/nn.4604.

C9orf72 Expansion Disrupts ATM-mediated Chromosomal Break Repair

Callum Walker[1,2,3,¶], **Saul Herranz-Martin**[2,¶], **Evangelia Karyka**[1,2,3], **Chunyan Liao**[3], **Katherine Lewis**[2], **Waheba Elsayed**[3,4], **Vera Lukashchuk**[2], **Shih-Chieh Chiang**[3], **Swagat Ray**[3], **Padraig J. Mulcahy**[2], **Mateusz Jurga**[3], **Ioannis Tsagakis**[2], **Tommaso Iannitti**[2], **Jayanth Chandran**[2], **Ian Coldicott**[2], **Kurt J. De Vos**[2], **Mohamed K. Hassan**[3,4], **Adrian Higginbottom**[2], **Pamela J. Shaw**[2], **Guillaume M. Hautbergue**[2], **Mimoun Azzouz**[1,2,*,#], and **Sherif F. El-Khamisy**[1,3,4,*,#]

[1]SITraN and Krebs Institutes, Neurodegeneration and Genome Stability Group, University of Sheffield, UK

[2]Sheffield Institute for Translational Neuroscience, University of Sheffield, 385a Glossop Road, S10 2HQ, Sheffield, UK

[3]Krebs and Sheffield Institutes for Nucleic Acids, Department of Molecular Biology and Biotechnology, Firth Court, University of Sheffield, S10 2TN, Sheffield, UK

[4]Center for Genomics, Helmy Institute for Medical Sciences, Zewail City of Science and Technology, Giza, Egypt

Abstract

A hexanucleotide repeat expansion represents the most common genetic cause of amyotrophic lateral sclerosis (ALS) and frontotemporal dementia, though the mechanisms by which the expansion cause neurodegeneration are poorly understood. We report elevated levels of DNA/RNA hybrids (R-loops) and double-strand breaks (DSBs) in rodent neurons, human cells, and in *C9orf72-ALS* patient spinal cord tissues. Accumulation of endogenous DNA damage is

[*]Correspondence should be addressed to Sherif El-Khamisy (s.el-khamisy@sheffield.ac.uk), Tel. +44 (0) 114 2222 791 and Mimoun Azzouz (m.azzouz@sheffield.ac.uk), Tel. +44 (0) 114 2222 238.
[¶]Joint first authors
[#]Joint senior authors made equal contribution

Author contributions

C.W conducted the immunocytochemistry, immunohistochemistry and immunoblotting experiments. S.H.M generated the mouse model and conducted behavioural experiments with assistance from K.L., V.L., T.I., J.S.C, and I.C. E.K and S.H.M. generated neuronal cell cultures. E.K, S-C.C, M.J, S.R., M.H. assisted with cell culture, imaging and DNA repair assays. K.L., V.L., T.I., I.C assisted with mouse experiments. C.L purified and conducted TOP1cc assays. K.D.V, I.T, J.C, A.H generated expansion constructs. I.T. and S.H.M. generated and validated viral vector stocks. W.E. optimised and conducted the neutral comet assays. P.J.S. and A.H. provided RRE constructs and I.T., J.S.C. and P.J.M. sub-cloned them into viral vectors. P.J.S. and A.H. provided the C9orf72-ALS biosamples and expertise. S.F.E-K, M.A, G.H, C.W, S.H.M analysed the data. S.F.E-K and C.W. wrote the manuscript with help from M.A. and S.H.M. All authors contributed to the final manuscript. S.F.E-K and M.A. conceived and co-led the project.

Data availability

The data that support the findings of this study are available from the corresponding authors upon reasonable request.

Competing financial interest

The authors declare no competing financial interest

Europe PMC Funders Author Manuscripts

concomitant with defective ATM-mediated DNA repair signalling and accumulation of protein-linked DNA breaks. We further reveal that defective ATM-mediated DNA repair is a consequence of p62 accumulation, which impairs H2A ubiquitylation and perturbs ATM signalling. Adeno-associated virus-mediated expression of C9*orf*72-related RNA and dipeptide repeats in the murine central nervous system causes elevated DSBs, ATM defects, and triggers neurodegeneration. These findings identify R-Loops, DSBs, and defective ATM-mediated repair as pathological consequences of *C9orf72* expansions, and suggest that *C9orf72*-linked neurodegeneration is driven, at least in part, by genomic instability.

Short tandem nucleotide repeats and microsatellites are common features of mammalian genomes. Expansion of a hexanucleotide G4C2 repeat in the non-coding region of chromosome 9 open reading frame 72 (*C9orf72*) is the most common genetic cause for amyotrophic lateral sclerosis (ALS) and frontotemporal dementia (FTD). Growing evidence suggests that *C9orf72* repeat expansions also contribute to a wide spectrum of neurodegenerative diseases such as Alzheimer's, Huntington's, multiple sclerosis, Parkinson's disease and cerebellar ataxias1. Approximately half of non-pathogenic *C9orf72* alleles possess two G4C2 repeats and the remaining half ranges from 2 to 25 repeats2. The pathogenic expanded repeat length, on the other hand, varies from tens to thousands3. *C9orf72* expansions are bidirectionaly transcribed leading to the formation of intracellular sense and antisense RNA repeat expansion foci (RRE). Moreover, the transcripts are prone to repeat-associated non-ATG (RAN) translation producing dipeptide repeat proteins (DPRs). Although a molecular understanding of *C9orf72* pathological phenotypes are beginning to emerge, the mechanisms by which the G4C2 repeat expansions cause ALS/FTD are not clear.

During the transcription of repetitive sequences, the nascent RNA is prone to hybridisation with the DNA template strand, displacing the complementary DNA strand and producing a three-stranded nucleic acid structure called R-loops4. R-loops primarily occur at GC-rich transcription sites, since guanine-rich RNA: cytosine-rich DNA hybrids are thermodynamically more stable than the respective DNA: DNA duplex5. Once formed, R-loops can be very stable structures, as they are bound together by Watson-Crick base pairing. These transcription by-products are a major threat to genome stability, since they are prone to DNA breakage6. Given the pure GC nature of the *C9orf72* repeat expansions and their propensity to form R-loops *in vitro*7, we hypothesised that R-loop-mediated genome instability may play a role in neurodegeneration linked to *C9orf72* repeats. To test this, we transfected MRC5 cells with 10 or 102 RREs and visualised R-loops using R-loop specific S9.6 antibodies. We concomitantly visualised RNA foci using fluorescence in situ hybridization (FISH). Expression of 102 RREs led to prominent RNA foci and triggered an approximate 7-fold increase in R-loop levels compared to cells transfected with a shorter expansion containing 10 RREs, which also displayed fewer RNA foci (Fig. 1a, $p=0.009$). Interestingly, R-loops and RNA foci co-localised in cells expressing 102 RREs, suggesting a physical relationship. The R-loop signal was specific since it disappeared following addition of RNAse H1, an R-loop specific resolvase (Fig. 1a).

We next evaluated the role of poly-GA DPRs in mediating R-loop formation. Transfection of MRC5 cells with either 34 or 69 DPRs revealed a length-dependent predisposition to dipeptide aggregates, in which DPRs were more abundant in cells transfected with 69 DPRs (Fig. 1b). Expression of 34 DPRs led to ~4 R-loop foci per cell and expression of 69 DPRs led to ~8 R-loop foci per cell, both of which were considered statistically higher than in control cells (Fig. 1b, p=0.046 and p=0.003, respectively), but were not statistically distinct from each other (Fig. 1b, p=0.1). These observations suggest that C9*orf*72 RNA-repeat expansions and poly-GA DPRs cause an increase in R-loop formation. To test if this is also true in *bona fide* post-mitotic neurons, we transduced rat cortical neurons with adeno-associated serotype 9 (AAV9) viral particles expressing 10, 102 RREs (Fig. 1c) or 34, 69 DPRs (Fig. 1d). Similar to human cells, expression of 102 RREs led to increased R-loop foci compared to control cells and cells transduced with 10 RREs (Fig. 1c, $p=0.018$). Likewise, 34 or 69 DPR expression increased the number of R-loop foci (Fig. 1d; p=0.001; p=0.0002, respectively), though the difference between 34 and 69 was not statistically significant (Fig. 1d, p=0.07). Together, these data show that G4C2 repeat expansions and poly-GA DPRs cause R-loop formation in mammalian cells.

Persistent accumulation of R-loops causes DNA double-strand break (DSB) formation and genome instability8. To test whether G4C2 repeat expansions cause DSBs we co-transfected MRC5 cells with 10, 102 RREs alongside GFP and examined DNA DSBs by immunostaining using antibodies for γH2AX (Ser-139 phosphorylated histone H2AX), an established marker for DSBs. As anticipated, expression of 102 RREs led to a significant increase in the number of cells exhibiting more than 10 γH2AX foci, when compared to control cells and cells expressing 10 RREs (Fig. 1e, p=0.005). Direct quantification of DSBs using the neutral comet assay revealed a similar increase in 102 RRE transfected cells compared to controls (Fig. 1f, p=0.006). Similarly, 34 or 69 DPR expression caused a significant increase in DSBs compared to controls, as measured by γH2AX immunostaining and the neutral comet assay (Fig. 1g, p=0.001; Fig. 1h, p=0.0003, respectively).

We next speculated that R-Loops might drive the formation of DSBs in cells expressing *C9orf72* repeat expansions. To directly test this hypothesis, we first assessed whether the elevated levels of R-Loops observed in *C9orf72* cells could be reduced by overexpressing the R-Loop resolution helicase, senataxin (SETX)9. Whilst control adenovirus expression of RFP had no detectable impact on R-loops, expression of SETX from the same viral backbone led to a marked reduction of R-Loop foci (Fig 1i,j, *left*). Overexpression of SETX, but not RFP, also reduced the number of γH2AX-positive cells (Fig. 1i, p=0.01; Fig 1j, p=0.022), indicating that R-Loops are a major source of *C9orf72* expansion-driven DSBs. Furthermore, SETX expression was able to reduce RRE- and DPR-driven cellular toxicity, as shown by a reduction in the % of cleaved-PARP1-positive cells (Fig. 1k,m; p=0.009 and p=0.038, respectively) and by a similar reduction in the % of Trypan Blue-positive cells (Fig. 1l,n; p=0.037 and p=0.025, respectively). The effect of SETX was specific to RRE-102- and 69-V5-positive cells since it did not impact cell viability in control cells expressing RRE-10 or 0-V5 constructs (Fig. 1k-n; p>0.05). Taken together, our data demonstrate that *C9orf72* repeat expansions promote R-Loop-driven DSB formation, which contributes to cellular toxicity.

The growing evidence that links *C9orf72* repeat expansions to cerebellar ataxias10,11 prompted us to test whether the activation of the master DNA repair kinase, mutated in ataxia telangiectasia (ATM), is dysregulated in cells expressing *C9orf72* expansions. Upon DNA breakage, ATM becomes activated in a process that involves its autophosphorylation at multiple sites, including serine 1981. This then sets in motion a cascade of downstream events resulting in 53BP1 recruitment and DNA repair12–14. While control cells displayed an average of 2 phosphorylated ATM (pATM) foci per nucleus, cells expressing DPRs (Fig. 2a, p=0.002) or 102 RREs (Fig. 2b, p=0.008) consistently possessed no, or in a few cases only one, focus. The reduced number of pATM foci is unlikely to be due to reduced ATM expression, as shown by Western blotting (Fig. 2c). It was also not due to an artefact of expressing the V5 epitope tag or transfection associated toxicity, since transfection with a V5 empty plasmid or GFP did not result in defective ATM signalling (Supplementary Figure 1). Since the accumulation of oxidative and protein-linked DNA breaks (PDBs) has been shown to cause neurodegeneration in man15–17, we next examined if pATM foci would form normally following exposure to the topoisomerase I poison camptothecin (CPT) or tert-butyl hydroperoxide (TBH); inducers of PDBs and oxidative DNA breaks, respectively. Treatment with CPT or TBH led to prominent increase in pATM foci in control cells (Fig. 2d). In a marked contrast, cells expressing 34, 69 DPRs (Fig. 2d) or 102 RREs (Fig. 2e) were unable to respond to DNA damage to the same extent, consistently showing less pATM foci. We conclude from these experiments that the expression of *C9orf72*-related DPRs and RREs impairs ATM activation.

An important consequence of defective ATM signalling is the defective accumulation of non-homologous end-joining (NHEJ) repair factors, such as 53BP1, into nuclear foci18. As expected, expression of 34 or 69 DPRs led to a marked reduction in 53BP1 recruitment to nuclear foci when compared to control cells (Fig. 3a, p=0.002). As was the case for pATM, this was not an artefact of expressing the V5 epitope-tag used to visualise DPRs, nor was it due to transfection-related toxicity, as it was not observed in cells transfected with vectors encoding V5 or GFP (Supplementary Figure 2a). Consistent with defective ATM in DPR expressing cells, pre-treatment with the ATM inhibitor Ku55933 significantly impaired 53BP1 foci formation in control cells but not in cells expressing 34 or 69 DPRs (Supplementary Figure 2c,d). As observed with DPRs, expression of 102 RREs also led to the suppression of 53BP1 foci formation, when compared to mock transfected cells and cells expressing 10 RREs (Fig. 3b, p=0.035). Strikingly, whilst CPT induced a significant increase in 53BP1 foci in control cells (Fig. 3c, p=0.009), expression of 34 or 69 DPRs prevented the CPT-induced increase in 53BP1 foci formation (Fig. 3c, p=0.294). Similarly, expression of 102 RREs prevented the CPT-induced increase in 53BP1 foci formation (Fig. 3d, p=0.496). To test if this was also true in *bona fide* post-mitotic neurons, we transduced rat cortical neurons with AAV9 viral particles expressing 34, 69 DPRs or 10, 102 RREs and examined 53BP1 foci formation following exposure to CPT (Fig. 3e,f). Consistent with results using MRC5 cells, whilst control neurons exhibited ~8 53BP1 foci, those expressing 69 DPRs or 102 RREs showed 3 or 1 foci per cell, respectively (Fig. 3 e,f, p<0.01). Consistent with our transfection data, this was not an artefact of viral transduction as cells transduced with AAV9 encoding V5 or GFP vectors possessed normal level of 53BP1 foci (Supplementary Figure 2b). Together, these data demonstrate that the expression of *C9orf72*-

related RREs or DPRs suppress 53BP1 recruitment to DSBs. To test whether the expression of *C9orf72*-related products results in defective phosphorylation of downstream ATM-effector proteins, we next examined the phosphorylation of p53, a known ATM target19. Whilst control cells displayed ~6-fold elevation of p-p53 levels in response to CPT treatment (Fig. 3g, p=0.037), cells expressing 34 or 69 DPRs showed no significant increase above baseline levels (Fig. 3g, p>0.05). Consistent with the 53BP1 data, we also observed a defect in the recruitment of p-p53 to nuclear foci in DPR expressing cells, which was mimicked in control cells by pre-treatment with the ATM inhibitor (Supplementary Figure 2e). Notably, ATM inhibition did not further attenuate p-p53 signalling in DPR-positive cells (p=0.059 and p=0.49 for 34 and 69 DPRs, respectively). Similarly, cells containing 102 RREs failed to induce p53 phosphorylation following CPT exposure (Fig. 3h, p=0.536), whilst mock-transfected cells and those expressing the 10 RREs did show increased p-p53 response to CPT treatment (Fig. 3h; p=0.0143 and p=0.01, respectively). Finally, in order to gain further evidence for defective ATM signalling, we next examined the accumulation of topoisomerase I (TOP1) – mediated PDBs, known as DNA covalent complexes (TOP1cc). ATM deficiency in primary neural cultures and in rodent models has been shown to cause elevated levels of TOP1cc, interfering with transcription and contributing to neuronal cell death20,21. Consistent with an ATM defect, cells expressing *C9orf72*-related DPRs or RREs exhibited ~4-fold increase in TOP1cc levels compared to controls (Fig. 3i). Taken together, these experiments reveal that *C9orf72*-related DPRs or RREs cause defective ATM signalling.

To further confirm ATM deficits in primary neural cultures we took advantage of the observations in *Atm* knockout mice and Ataxia Telangiectasia (A-T) patient tissue in which histone deacetylase 4 (HDAC4) is abnormally localised to the nucleus of neurons22. To remain cytoplasmic, HDAC4 requires sustained phosphorylation, which is maintained by an intricate balance between phosphorylation and dephosphorylation. The latter is conducted by protein phosphatase 2A (PP2A), the activity of which is negatively regulated by ATM. Thus, ATM deficiency results in increased PP2A activity, leading to HDAC4 hypophosphorylation and, in turn, its re-localisation to the nucleus. HDAC4 knockdown/inhibition and cytoplasmic HDAC4 conferred therapeutic benefit *in vitro* and *in vivo* models of A-T22. To test if the ATM deficits triggered by *C9orf72*-related DPRs would also cause nuclear accumulation of HDAC4, we transduced rat cortical neurons with AAV9 viral particles expressing 69 DPRs and examined the cellular localisation of HDAC4. Whilst HDAC4 appeared cytoplasmic in control neurons, it showed marked nuclear enrichment in neurons expressing 69 DPRs with no detectable change in neuronal morphology (Supplementary Figure 3a,c). Subsequent quantification revealed ~3 fold increase in nuclear HDAC4 driven by 69 DPR expression (Supplementary Figure 3b, p=0.001). Nuclear accumulation of HDAC4 was not an artefact of viral transduction as neurons transduced with AAV 9 encoding V5 epitope tag or GFP displayed normal cytoplasmic HDAC4. Furthermore, pre-treatment of primary neurons with an ATM inhibitor (Ku 55933) similarly caused nuclear HDAC4 re-localisation (Supplementary Figure 3d,e), suggesting that the observed phenotype is due to ATM deficit.

We next examined if these observations were also true *in vivo*. To achieve this, AAV9 viral vectors encoding 10, 102 RREs, or 0, 69 V5-tagged DPRs were delivered into the

cerebrospinal fluid via cisterna magna of wild type mice at post-natal day 1 (P1), which led to transgene expression in multiple areas of the CNS (Supplementary Figure 4). As was the case *in vitro*, expression of 102 RREs or 69 DPRs in mouse CNS tissue, led to HDAC4 nuclear re-localisation and accumulation of DSBs as measured by increased γH2AX foci (Fig. 4a-d, $p<0.05$). We next tested if the pronounced DNA repair defect observed *in vivo* would lead to neuronal cell death. Brain extract from mice injected with 69-V5 DPRs displayed ~2-fold increase in PARP1 cleavage compared to mice injected with 0-V5 DPRs (Fig. 4 e, $p=0.045$). To further confirm the loss of neuronal cells in CNS tissue derived from mice expression DPRs, we used NeuN immunohistochemistry to quantify neurons from brainstem sections. Consistent with our Western blotting data, we observed ~20% reduction in neurons from brainstem sections derived from mice injected with 69 DPRs when compared to mice injected with 0-V5 (Fig. 4f; $p=0.048$). Given the loss of neuronal cells, we anticipated that this would translate into a gross functional motor deficit at the whole organismal level. Indeed, aged 6 months, DPR injected mice consistently displayed an aberrant stand, swing speed and stride length, when analysed using a catwalk gait system (Fig. 4 g, $p<0.01$). At 12 months, we assessed the hind limb splay of these mice using a manual scoring system. DPR injected mice also displayed an increase in hind limb splay (Supplementary Figure 5, $p<0.01$). Taken together, these data demonstrate the expression of *C9orf72*-related RREs or DPRs cause ATM defects and DSBs in the murine nervous system, and that these observations are linked to a neurodegenerative phenotype in mammals, which is also consistent with the neurological deficits triggered by 50 poly-GA DPRs reported recently23.

After showing that poly-GA expression causes ATM dysfunction and neurodegeneration in mice, we next set out to get more insight into the molecular mechanism of the ATM defect. In response to DNA damage, ATM signalling is mediated by the MRN complex, which forms foci at sites of DSBs, facilitating interactions between ATM and Nbs124, and thereby enhancing ATM phosphorylation. Thus, we speculated that defective ATM signalling might be a consequence of upstream Nbs1 disruption. In contrast to 53BP1 and pATM, Nbs1 foci formed normally in DPR expressing cells (Fig. 5a). Similar to γH2AX, expression of 69 DPRs led to an increase in Nbs1 foci formation (Fig 5a, $p=0.001$). These data argue against the failure of Nbs1 recruitment as a cause for the *C9orf72*-related ATM defect.

Central to efficient ATM mediated signalling is a cascade of post-translational histone modifications required for efficient and sustained DSB repair. An important event is the ubiquitylation of histone H2A by the E3 ubiquitin ligase RNF168, which plays an important role for the recruitment of 53BP1 to DSBs25–29. Importantly, RNF168 mediated H2A ubiquitylation, and subsequent 53BP1 recruitment, has also been shown to maintain efficient ATM signalling30,31. We thus examined if *C9orf72* expansions would impact H2A ubiquitylation, which may explain the observed ATM signalling defect. Consistent with previous reports27–29, Western blot analyses using H2A specific antibodies revealed multiple ubiquitylated species (Fig 5b). The extent of H2A ubiquitylation, however, was attenuated in DPR expressing cells, which showed ~ 2-fold less H2A ubiquitylation in comparison to controls (Fig 5b, $p= 0.0042$). Consistent with the Western blotting data, immunostaining with specific ubiquitylated-H2A (ub-H2A) antibodies also revealed reduced levels of ub-H2A foci in cells expressing 69 DPRs, when compared to control cells (Fig. 5c,

p=0.013). Interestingly, although DPR-positive cells exhibited fewer ub-H2A foci, we noticed co-localisation between DPRs and ub-H2A (Fig 5c, arrow). Since RNF168 is the key ubiquitin ligase driving H2A ubiquitylation32, we wondered if the defective ATM signalling is due to decreased availability of RNF168. Consistent with this idea, increasing the pool of RNF168 by overexpression of GFP-RNF168 in DPR expressing cells restored 53BP1 (Fig 5d, *p=0.0003*) and increased pATM (Fig 5e, *p=0.006*) foci formation. Moreover, these experiments revealed that RNF168 was also sequestered into DPRs (Fig 5d, arrow), explaining the unexpected co-localisation between DPRs and ub-H2A.

Inspired by a recent seminal report showing that the ALS-associated autophagy protein, p62/SQSTM1, perturbs RNF168 function and impairs H2A ubiquitylation-mediated DNA repair33, we wondered if the defective ATM signalling in *C9orf72* models may result from a p62-mediated attenuation of H2A ubiquitylation. This hypothesis is particularly attractive since p62 accumulation is a hallmark pathology of *C9orf72*-related disease34,35. If this is true, we predicted that depletion of p62 in DPR expressing cells would recapitulate the effect of RNF168 overexpression. Indeed, p62 depletion with siRNA (Fig 5f) led to restoration of 53BP1 (Fig 5g, *p=0.047*) and pATM (Fig 5h, *p=0.003*) foci. These data are fully in-line with reports that p62 accumulation impairs RNF168-mediated H2A ubiquitylation33 and with studies that highlight the role of H2A ubiquitylation in ATM signalling30,31. Furthermore, the restoration of ATM-mediated repair in DPR-positive cells by p62 depletion suppressed the number of DSBs (Fig. 5i, *p*=0.029) and the aberrant accumulation of R-loops (Fig. 5j, *p*=0.0.037). The latter is consistent with the recently reported reciprocal functional interaction between R-loops and ATM signalling36,37. The above data suggest that p62 accumulation and the consequential defect in ATM signalling act together with the expansion-driven R-loops to trigger genome instability, though it is not clear whether they constitute distinct or epistatic pathways. To address this question, we examined whether SETX overexpression would further suppress the elevated level of DSBs in p62-depleted cells. Consistent with our previous data (Figure 1j and Figure 5i), overexpression of SETX or depletion of p62 was capable of reducing γH2AX foci in DPR-positive cells (Fig. 5k; *p*=0.0013 and 0.0146, respectively). However, the concomitant overexpression of SETX and depletion of p62 further reduced DSB levels compared to levels observed by SETX overexpression or p62 depletion alone (Fig. 5k; *p*=0.0433 and *p=0.0045*, respectively) Together, these data identify two separate arms that drive genome instability in DPR expressing cells. One arm is driven by p62 accumulation, defective H2A ubiquitylation and the subsequent ATM signalling defect; and the other is driven by repeat-associated R-loop accumulation. Whilst the two arms are distinct, cross-talk does exist due to the reciprocal functional interaction between R-loops and ATM signalling36,37.

In addition to DNA damage, ATM can also become activated in the absence of DNA damage by the drug chloroquine, a DNA intercalating agent38. Since the accumulation of p62 and inhibition of H2A ubiquitylation led to dysfunctional ATM signalling in *C9orf72* cells, we reasoned that ATM activation by chloroquine, which is not linked to sensing DNA damage, would not be defective. Thus, we tested whether chloroquine-induced chromatin relaxation could restore ATM signalling in DPR-positive cells. As predicted, whilst DPR-positive cells did not display any ATM phosphorylation under normal conditions, chloroquine treatment led to pan-nuclear ATM phosphorylation (Supplementary Figure 6a, *p=0.004*), indicating

that DPR expressing cells are indeed responsive to chloroquine and, consequently, are able to activate ATM. To test whether the ensuing ATM signalling was restored by chloroquine treatment in *bona fide* primary neuronal cells, we next examined the localisation of HDAC4, which we previously demonstrated is localised to the nucleus of neurons expressing DPRs. As predicted, whilst DPR-positive neurons displayed nuclear HDAC4, the addition of chloroquine led to re-localisation of HDAC4 to the cytoplasm (Supplementary Figure 6b). Whilst only ~40% of DPR-positive neurons displayed cytoplasmic HDAC4 without chloroquine treatment, the number of neurons with cytoplasmic HDAC4 increased to almost 100% after cell treatment with chloroquine (Supplementary Figure 6b; p=0.014). These data demonstrate that ATM can be activated by inducing chromatin relaxation, and are consistent with our previous data linking dysfunctional ATM signalling to a defect in histone ubiquitylation.

Given that chromatin compaction has been reported in *C9orf72* samples39, we speculated that an increase in heterochromatin formation might be a hallmark of *C9orf72*-DPR expressing cells. Using H3K9me3 as a marker for heterochromatin, we confirmed that DPR expression increases heterochromatin formation, as measured by ~50% increase in H3K9me3 signal by western blotting and immunocytochemistry, in comparison to empty vector control cells (Supplementary Figure 7a,b, p=0.002). Since ATM has been linked to the repair of heterochromatic DSBs40, we wondered if promoting chromatin relaxation by Trichostatin A (TSA)41,42 would reduce DSBs levels in DPR-positive cells. Indeed, treatment of DPR-positive cells with TSA led to a reduction of H3K9me3 nuclear fluorescence (Supplementary Figure 7c, p=0.002). Unlike chromatin relaxation by chloroquine, TSA treatment did appear to activate ATM signalling (Supplementary Figure 7c). TSA treatment did, however, lead to a reduction in γH2AX – but not R-Loop - foci in DPR-expressing cells (Supplementary Figure 7d,e, p=0.001), suggesting that chromatin relaxation reduces DSB levels by decreasing the requirement for ATM signalling, rather than activating ATM directly. This is in-line with the reported role of ATM during the repair of heterochromatic DSBs, in which the DNA repair deficit caused by ATM inhibition was similarly overcome by chromatin relaxation40. Importantly, TSA treatment increased DSB levels in control cells, suggesting that whilst TSA is beneficial in *C9orf72* models in which the chromatin is compact, it may confer sensitivity to other types of DNA lesions in cells with non-pathological chromatin arrangements41. Finally, we wondered whether TSA treatment would also have beneficial effects on cell survival in *C9orf72* models, as a result of reduced DSBs. TSA treatment was able to rescue the cell toxicity triggered by 69 DPR expression to a similar level that was observed in DMSO treated control cells, as measured by both PARP1 cleavage (Supplementary Figure 7f, p=0.0004) and trypan blue exclusion assays (Supplementary Figure 7g, p=0.003). These data suggest that *C9orf72*-related DPRs drive the formation of heterochromatin, thereby exacerbating the ATM defect and ultimately leading to cell death.

Next, we set out to understand why *C9orf72* cells display increased heterochromatin formation. Whilst R-loops are generally associated with euchromatin, their progressive accumulation may also drive heterochromatin formation43,44. As such, we hypothesised that increased heterochromatin might be, at least in part, caused by the expansion-driven R-loops. SETX overexpression was able to reduce heterochromatin levels in DPR-positive cells

(Supplementary Figure 7h, p=0.031). Additionally, SETX overexpression did not further reduce DSBs in TSA treated *C9orf72* cells (Supplementary Figure 7i). Since ATM signalling is particularly important for the relaxation and subsequent repair of heterochromatic DNA35, we speculated that increased heterochromatin might also be a consequence of *C9orf72*-linked ATM dysfunction. We observed a reduction in H3K9me3 signal after restoring ATM signalling with p62 siRNA (Supplementary Figure 7j, p=0.025). Similarly, the reduction of DSBs via p62 depletion appeared to be epistatic with TSA treatment (Supplementary Figure 7k). Taken together, these data demonstrate that chromatin relaxation via TSA attenuates heterochromatin levels, genomic instability, and cellular toxicity in *C9orf72* models. We propose a model in which *C9orf72* repeat expansion drive the formation of heterochromatin, placing greater demand on ATM-mediated repair - a system that is already defective – and thereby creating a vicious cycle that leads to neuronal cell death. Although this is an attractive model for *C9orf72* pathologies, we note that TSA can enhance DNA damage sensitivity in *C9orf72* unrelated models41,45, suggesting that the extent of heterochromatin and genome-wide distribution of breaks greatly influence the response of mammalian cells to TSA.

Finally, we examined if R-loops, DNA breaks and defective ATM signalling observed in human cells, mouse neurons, and in mice were also present in *C9orf72*-ALS patient tissues. To test this, we subjected post-mortem spinal cord sections from controls and *C9orf72*-ALS patients to R-loop, γH2AX, and HDAC4 immunohistochemistry analyses. Consistent with our cellular data, we observed a significant increase in the number of R-loop (Figure 6a,b; *p=0.0038*) and γH2AX-positive motor neurons (Figure 6c,d; *p=0.0268*) in *C9orf72*-ALS sections compared to controls. The specificity of S9.6 signal was confirmed by prior treatment with RNAse H1 (Supplementary Figure 8). In addition, we also observed an increase in the percentage of motor neurons with nuclear HDAC4 staining in *C9orf72*-ALS sections compared to controls (Figure 6e,f, *p=0.0463*), suggesting that ATM signalling is also dysregulated in *C9orf72*-ALS patient motor neurons. We note that nuclear accumulation of HDAC4 could also result from other factors, such as increased activity of the inhibitor of PP2A (I2PP2A), which has been observed in sporadic-ALS patients46. We also observed an increase in H3K9me3 nuclear fluorescence in *C9orf72*-ALS motor neurons (Supplementary Figure 9, p=0.022). Together, our findings are consistent with a model whereby the expression of *C9orf72*-related products drive R-loop-mediated DNA breakage that is further exacerbated by the suppression of ATM-mediated DSB repair, resulting in disruption of co-transcriptional processing and neurodegeneration (Supplementary Figure 10).

In summary, we identified an increase in R-Loops and a defect in ATM signalling using 4 model systems: human cells, rodent neuronal cultures, RNA and dipeptide mouse models of *C9orf72*-related expansions, and in post-mortem ALS patient tissues. Consistent with an ATM defect, we further report increased accumulation of TOP1 mediated protein-linked DNA breaks (PDBs), an established marker for neurodegeneration20,21,47,48, in cells expressing *C9orf72*-related products. Furthermore, CNS tissues obtained from mice expressing *C9orf72*-related DPRs and from *C9orf72*-ALS patients exhibit nuclear HDAC4 retention, which is consistent with defective ATM signalling22. We further uncover an important link between pathological accumulations of p62 - a hallmark of *C9orf72*-ALS - and defective H2A ubiquitylation, dysfunctional ATM-mediated DNA repair, and increased

genomic breaks. Our data reinforce the pathophysiological significance of the recently reported mechanism by which p62 impedes DNA damage repair33. A length-dependent increase in R-loops was evident in cells expressing RREs, likely driven by G-rich RNA, which is prone to template strand invasion. Genome-wide analyses in yeast suggest that R-loops can regulate sense and antisense gene expression49, possibly explaining the aberrant expression of both transcript types in *C9orf72* patient samples50. Notably, suppressing R-loop levels by SETX overexpression was able to reduce DSBs and cellular toxicity in both RRE and DPR models of *C9orf72*-related disease.

To conclude, we uncover two distinct but partially overlapping pathways by which *C9orf72* repeat expansions lead to genomic instability. One arm is driven by p62 accumulation, defective H2A ubiquitylation and defective ATM signalling, as measured by impaired 53BP1 foci formation and the phosphorylation of downstream target p53, the accumulation of TOP1 mediated PDBs, and nuclear accumulation of HDAC4. The second arm is driven by the expansion led increase in R-loop formation. Increased R-Loops and defective ATM signalling can account for multiple yet unexplained phenotypes of *C9orf72* repeat expansions: (**1**) increased heterochromatin, (**2**) increased DSBs, and (**3**) the previously reported *C9orf72*-associated splicing defects37. Finally, this work suggests that targeted modulation of R-Loop homeostasis by R-Loop specific helicases, or DSB repair kinetics by chromatin modulating drugs, may offer new therapeutic opportunities for C9*orf*72-related neuropathologies.

Methods

Mammalian Cell Culture

MRC5 cells were grown in Minimum Essential Media (MEM) (Sigma Aldrich) supplemented with 10% Foetal Bovine Serum (FBS) (Sigma Aldrich), 2mM L-Glutamine (Sigma Aldrich) and 1% Penicillin/Streptomycin (Sigma Aldrich). HEK 293T cells were grown in Dulbecco's Modified Essential Media (Sigma Aldrich) supplemented with 10% Foetal Bovine Serum (FBS), and 1% Penicillin/Streptomycin (Sigma Aldrich). MRC5 cells were seeded on coverslips into the wells of a 24-well plate at a density of 3 x 10^5 cells/cm^2. For other experiments, HEK 293T cells were seeded into the wells of a 12-well plate at a density of 3 x 10^5 cells/cm^2. The following day, cells were transfected with 250ng of DNA/cm^2 of each DNA plasmid, using polyethylenimine at a molar concentration of 3:1 (PEI: DNA). 6-hours post-transfection, the media was replaced and cells were incubated for a further 2 or 3 days, as indicated in the figure legends. For p62 knockdown experiments, MRC5 cells were co-transfected with cDNA plasmids using PEI (as described above) alongside control siRNA particles or p62 targeting particles (Santa Cruz, sc-29679) at a molarity of 25nm. Dharmafect was used as the transfection reagent for all siRNA experiments at a ratio of 1:1 (siRNA:Dharmafect). Recombinant adenovirus (Adenovirus-type 5 dE1/E3) encoding for SETX or RFP were purchased from Vector Biolabs. Viral stocks (10^9) were diluted 1:5000 for MRC5 and 1:20000 for HEK293T cells to give an approximate multiplicity of interest (MOI) of 10 and 2.5 for MRC5 and HEK 293T cells, respectively. Virus containing media was added for 2-3 hours, prior to transfection, and replaced with fresh. For Western blotting, cell death assays, and COMET assay experiments,

MRC5 cells and HEK 293T cells were grown for 72 hours post-transfection. For DNA repair immunocytochemistry assays, cells were grown for 48 hours post-transfection.

Generation of Repeat Expansion Constructs

Synthesised TCGAC$(G4C2)_{10}$ sense and ACGT$(G2C4)_{10}$ antisense ssDNA oligonucleotides (Sigma-Aldrich) were designed with SalI/XhoI overhangs. The dsDNA oligos were generated by denaturing oligos were denatured at 99ºC for 30 min and then annealing by stepwise cooling of 0.5ºC/min. These $(G4C2)_{10}$ were ligated into SalI and XhoI digested pcDNA6.2-GW/EmGFP-miR (Invitrogen), to generate pcDNA6.2-GW/EmGFP-$(G4C2)_{10}$. Further $(G4C2)_{102}$ repeats were subcloned using the 3' XhoI site. pCMV-EmGFP-(G4C2)n vectors containing 10 and 102 repeats were generated via this method. EmGFP was subsequently excised using the flanking DraI restriction site. The $(G4C2)_{10}$ and $(G4C2)_{102}$ constructs were sub-cloned into pcDNA5/FRT/TO HIS (Addgene) using DraI and XhoI restriction sites. Transformations of plasmids containing the (G4C2)n repeat constructs were performed using recombination-deficient β-10 E.coli (NEB) to minimise (G4C2)n repeat shrinkage. To model gain-of-function via RAN translation of C9orf72 repeat expansions we produced two expression constructs coding for uninterrupted V5-tagged poly-GA DPRs, using an expandable cloning strategy with Age1 and Mre1 as compatible enzymes51. We first constructed a 'start acceptor' pCi-Neo vector (Promega) by cloning a V5-3xGA insert into the Xho1/Not1 sites (ctc gag gcc acc atg ggc aaa ccg att ccg aac ccg ctg ctg ggc ctg gat agc acc ggt gca ggt gct ggc gcc ggc gga tcc gaa ttc tag ccg cgg ccg c) and a 'start donor' vector with a 14xGA insert (ctc gag acc ggt gca ggt gct gga gct ggt gca ggt gct gga gca ggt gca ggt gct gga gct ggt gca ggt gct gga gca ggt gct ggc gcc ggc gga tcc gaa ttc ccg cgg ccg c) in the Xho1/Not1 sites and used these to propagate the GA repeats as shown below to construct 34, 69 GA repeats. A V5 construct that lacked DPRs was created by AgeI and NGOMIV digestion, which excised the DPR coding region.

Primary Cortical Neuron Cultures

The cortex from the brains of E17.5 rat pups were harvested and stored in Hank's Balanced Salt Solution (without calcium, without magnesium) (HBSS -/-) (Sigma Aldrich). The tissue was washed with HBSS (-/-) and then incubated with 0.0035% Trypsin (Sigma Aldrich) for 15 minutes. DNAse (10μg/mL)(Sigma Aldrich) was then added at a ratio of 1:1 (v/v), and the tissue was re-suspended in 1mL triturating solution (1% Albumax, 25mg Trypsin Inhibitor, 10μg/mL DNAse) (Sigma Aldrich). Neurobasal media (ThermoFisher), supplemented with 2 mM L-Glutamine (Sigma Aldrich), 1% Penicillin/Streptomycin (Sigma Aldrich) and 1 x B-27 (Sigma Aldrich) was then added at a ratio of 1:5 (Triturating solution:Neurobasal media). Cells were then plated onto Poly-D-Lysiene coated coverslips, in the wells of a 24 well-plate at a density of 9.365×10^4 cells/cm^2. 1.5×10^5 viral genomes (vg) per cell of AAV9 was added to cultures after 5 days *in vitro* (DIV). Half of the culture media was replaced with fresh media every 3 days. 7-days post-transduction (13 DIV), cells were treated with CPT (10μM) where indicated, and fixed using 4% paraformaldehyde or methanol:acetone (50:50).

Production of viral vectors

Sixty 15 cm plates containing HEK 293T cells at a 80% confluence were transfected using polyethylenimine (MW ~ 25K) with a mixture of three plasmids (at a molar ratio of 2:1:1 in order as listed) required to generate an infectious AAV9 viral particle: (1) a plasmid providing helper genes isolated from adenovirus that enhance viral infectivity (pHelper); (2) an ITR-containing plasmid plasmid containing the 10, 102 RRE or 34, 69 DPR driven by the CMV promoter; (3) a plasmid that carries the AAV Rep-Cap proteins (pAAV2/9); (3) A total of 52μg of DNA was transfected per plate with pHelper:pAV2-CMV-GFP:pAAV2/9. For all experiments, we used the pAV2-CMV-GFP consisting of two ITRs in a truncated genome that resulted in a self-complementary AAV9 (scAAV9). Four days after transfection, the AAV enriched media was collected, incubated at 37°C for 2 hours with 3,750 units of benzonase-nuclease (Sigma, USA), filtered through a 0.22 μm filter, and concentrated to a volume of 1ml using Amicon spin filter units (Millipore, USA). The virus was then washed with 50 ml of phosphate buffered saline (PBS, pH 7.3) in the same Amicon spin filter units, and concentrated to a final volume of 0.5 ml. The viral sample volume was expanded to 14ml with PBS and separated through a discontinous iodixanol (D1556, Sigma, USA) gradient (4ml of 54%, 9 ml of 40%, 9 ml of 25%, 5 ml of 15%), and centrifuged at 69,000 rpm for 1.5 hours at 18°C. The purified virus, which was found as a white layer between the 54% and 40% iodixanol gradient was subsequently removed in 0.5ml fractions using a syringe, and 10μl of each fraction was mixed at an equal ratio with a 2X reducing sample SDS-PAGE buffer, heated to 75°C for 20 minutes, separated on a 4-20% precast TGX mini-gel (Biorad, USA), and stained with Sypro-Ruby according to the manufacturer's protocol (Life Techologies, USA). Fractions that showed a pure virus composed solely of the VP1, VP2 and VP3 bands were combined, and washed against 5 full volumes (15ml each) of PBS with an Amicon spin filter, before collecting in a final volume of between 300-500μl. Concentrated viral stocks were stored at -80°C until usage.

Viral titers were determined with the Quantifast SyBR Green PCR Kit (Qiagen, Cat 204054) on a BioRad CFX96 thermal cycler, following the manufacturer's instructions. The number of GFP copies in three dilutions of a purified AAV9 virus (100x, 1000x, 10,000x) were compared to a standard curve generated by serial dilutions of a linearized pAV2-CMV-GFP vector. Primers used to quantify viral genomes were (Poly A, Forward: 5'-ATT TTA TGT TTC AGG TTC AGG GGG AGG TG-3'), (PolyA, Reverse: 5'-GCG CAG AGA GGG AGT GGA CTA GT-3'), (GFP, Forward: 5'- GAC GGC AAC ATC CTG GGG CAC AAG-3'), and (GFP, Reverse: 5': CGG CGG CGG TCA CGA ACT C-3').

RNA Fluorescent-In-Situ-Hybridisation (FISH)

FISH was performed following a modification of the method described previously52. MRC5 cells or rat cortical neurons were fixed with 4% PFA for 10 minutes at room temperature. For S9.6 staining however, fixation was performed using ice-cold methanol:acetone (50:50) for 10 minutes at -20°C. Cells were then incubated with pre-hybridisation buffer (50% formamide, 2X saline sodium citrate (SSC), 100 mg/ml dextran sulphate, 50 mM sodium phosphate pH 7.0) for 1 hour at 66°C. Subsequently, cells were incubated with hybridisation buffer containing a 5' TYE-563-labelled locked nucleic acid (16-mer fluorescent)-incorporated DNA probe against the GGGGCC RNA hexanucleotide repeat (Exiqon, Inc.,

batch number 607323), at a concentration of 400 ng/ml for 1 hour or overnight at 66°C. A 1 hour incubation period was preferred for phospho-ATM staining, due to the loss of antigen signal after overnight treatment in hybridisation buffer. After hybridization, slides were washed once in 2 X SSC with 0.1% Tween-20 at room temperature and three times in 0.1 X SSC at 66°C. All washes were performed for 10 minutes. All solutions were made with DEPC-treated water. Following the completion of this FISH protocol, ICC was then performed as described below, though using DEPC-treated PBS solutions.

Immunocytochemistry (ICC)

MRC5 cells or rat cortical neurons were fixed with 4% PFA for 10 minutes at room temperature, or with ice-cold methanol:acetone (50:50) for 10 minutes at -20°C. Cells were then washed 3 times with Phosphate Buffered Saline (PBS), incubated with 0.5% Triton-X (in PBS) for 5 minutes, and washed a further 3 times with PBS. In order to confirm the specificity of the S9.6 antibody, MRC5 cells, fixed with methanol:acetone, were incubated with RNASE H enzyme (100units/mL) in 3% BSA in PBS overnight at 4°C before ICC/FISH-ICC. For ub-H2A staining, cells were incubated with PBS containing 0.5% Triton-X for 2 minutes at room temperature before fixation with 4% PFA. Subsequently, cells were incubated with 3% BSA for 30 minutes, before being incubated with primary antibodies (in 3% BSA) for 1 hour (with the exception of Ub-H2A, which was incubated overnight at 4°C). For DPR experiments, a V5 antibody was always used to detect DPR-positive cells. Cells were washed 3x with PBS and incubated with fluorescent secondary antibodies (in 3% BSA) for 1 hour, before being washed another 3x with PBS. Coverslips were mounted onto glass slides using Fluoromount™ Aqueous mounting medium (Sigma Aldrich).

Anti-V5 antibodies: mouse (Abcam, ab27671), and rabbit (Bethyl, A190-120A) were used at 1:1000. A mouse anti-RNA:DNA hybrid (S9.6) antibody (Kerafast, ENH001) and a mouse anti-ub-H2a antibody (Merck Millipore, E6C5) were used used at a concentration of 1:500 for immunocytochemistry, and at 1:5000 for FISH-ICC double staining. A mouse anti-γH2AX (Ser 139) antibody (Merck Millipore, JBW301), a rabbit anti-53BP1 antibody (Bethyl, A300-272A), a rabbit anti-phospho-ATM antibody (Abcam, EP1890Y), a mouse anti-phospho-P53 antibody (Cell Signalling, 9286s), a mouse anti-cleaved PARP (Cell Signalling, 9548), and a rabbit anti-Nbs1 antibody (Sigma, N3162) were all used at a concentration of 1:1000. A rabbit anti-HDAC4 antibody (Abcam, ab1437) was used at a concentration of 1:250. A rabbit H3K9me3 antibody (Abcam, ab8898) was used at a concentration of 1:2000. Subsequently, cells were washed 3 times with PBS and incubated with the corresponding Alexa fluor secondary antibodies (all purchased from Life Technologies and used at a concentration of 1:500) as well as DAPI for 1 hour. For FISH-IF double staining, an Alexa fluor 488 was used in conjunction with the Cy3 fluorescent probe. Cells were washed a further 3 times with PBS and coverslips were mounted onto glass slides using Fluoromount™ Aqueous mounting medium (Sigma Aldrich).

Immunohistochemistry

Mouse brain and spinal cord sections were incubated with 0.5% Triton-X for 30 minutes, followed by a 1 hour incubation with 3% BSA (with 0.2% Triton-X) for 1 hour. Subsequently, sections were incubated with primary antibodies (in 3% BSA with 0.2%

Triton-X) overnight at 4°C. The following day, sections were washed 3 times with PBS, and were incubated with fluorescent secondary antibodies alongside DAPI for 1 hour at room temperature. For γH2AX and HDAC4 staining in DPR mice sections, a biotinylated secondary antibody was used in conjunction with a tertiary anti-streptavidin Alexa Fluor 488 antibody, in order to enhance the signal. Sections were washed a further 3 times, before mounting with Fluoromount™ Aqueous mounting medium (Sigma Aldrich). For human spinal cord staining, 5μm paraffin embedded spinal cord sections from *C9orf72*-ALS and non-ALS controls (Supplementary Table-1,) were incubated with primary antibodies specific for HDAC4 (Abcam, ab1437), γH2AX (R&D systems, AF2288), S9.6 (Kerafast, ENH001), or H3K9me3 (Abcam, ab8898) at concentrations of 1:250, 1:500, 1:1000 and 1:1000; respectively. The NeuN D3S3I antibody was from cell signalling (Cat no 12943) and was used at a concentration of 1 in 500. Before primary antibody incubation, antigen retrieval was performed in 10 mM Sodium citrate (pH6) or 10 mM Tris Base for HDAC4, S9.6 and H3K9me3, or 1 mM EDTA (pH9) for γH2AX. Antigen retrieval was performed for 30 minutes in a pressure cooker. Immunohistochemistry was performed using the intelliPATH FLX™ Detection Kit, according to the manufacturer's protocol. Work on human tissue was reviewed by the Sheffield Brain Tissue Bank (SBTB) Management Board and approved to release tissue under REC 08/MRE00/103 was granted. All post-mortem tissue stored at Sheffield Brain Tissue Bank was obtained with informed consent.

Cell Lysis, SDS-PAGE and Western Blotting

In order to collect whole-cell lysates, MRC5 cells, HEK 293T cells, or mice brain stem sections were lysed in RIPA buffer (150 mM NaCl, 0.5% sodium deoxycholate, 0.1% SDS, and 50 mM Tris, pH 8.0, supplemented with protease inhibitor cocktail, Sigma Aldrich) on ice for 30 minutes, before being sonicated in order to shear the DNA. For the isolation of chromatin fractions, the cytoplasmic and nuclear soluble proteins were first removed by hypotonic and hypertonic buffers. The remaining pellet was lysed with *nuclear insoluble buffer* (20mM Tris ph8, 150mM NaCl, 1% SDS, and 1% NP-40) for 30 minutes on ice before being sonicated. The protein concentration of each whole-cell lysate was estimated using a BCA assay (Pierce™), and equal quantities of protein were mixed with a 2X reducing sample SDS-PAGE buffer, heated to 95°C for 5 minutes, separated on a 4-20% precast TGX mini-gel (Biorad, USA), and transferred onto a PVDF membrane (Millipore, USA). Membranes were blocked with 3% BSA in TBS with 0.05% Tween (TBST) for 30 minutes, before incubating at either room temperature for 2 hours or 4°C overnight with agitation with primary antibody in 3% BSA in TBST. For Western Blotting, a mouse a rabbit ATM antibody (Abcam, ab82512) was used at 1:2000, a rabbit H3K9me3 antibody (Abcam, ab8898) was used at 1:5000, mouse anti-α Tubulin (Abcam, T9026) and mouse anti-GAPDH (Calbiochem, CB1001) were used at 1:5000. Cleaved-PARP antibodies (Cell Signalling, 9548) were all used at 1:1000. Rabbit anti-H2A antibodies (Abcam, ab18255) were used at 1:1000. Membranes were then washed 3 times for 5 minutes with TBST and incubated with either a HRP-linked secondary anti-mouse antibody (Bio-Rad, 1721011) or an anti-rabbit antibody (Dako, D048701-2). Enhanced ChemiLuminescence (ECL) substrate was then added to the membrane to enable detection, and non-saturated images were acquired using a G:BOX EF machine (Syngene) and Snapgene software (Syngene). Supplementary Figures 11-14 contain raw files of the Western blots used in this study.

Trypan Blue Cell Death Assay

3 days after transfection, HEK 293T cells were washed once with PBS and treated with trypsin until detached. Subsequently, 10% FBS-containing DMEM was added and cells were resuspended gently by pipetting up and down 3 times. Cell suspensions were then mixed with Trypan Blue (0.04%) at a ratio of 1:1. Immediately after, the percentage of cells that were permeable to Trypan Blue was calculated using a haemocytometer and a brightfield microscope. Scoring was performed under single-blinded conditions.

Measurement of topoisomerase I cleavage complexes (TOP1cc)

TOP1 protein–DNA complexes were purified using caesium chloride density gradients. Approximately $2x10^6$ cells were lysed in 1% sarcosyl, 8 M guanidine HCl, 30 mM Tris pH 7.5 and 10mM EDTA. Cell lysates were then incubated at 70°C for 15 minute to remove all non-covalently bound proteins from DNA. Cell lysates were then loaded on a caesium chloride density (CsCl) step gradient (5 ml total volume) and centrifuged at 75,600 × g at 25°C for 24 hour to separate free proteins from DNA. Ten consecutive 0.5 ml fractions were collected and slot blotted onto Hybond-C membrane (Amersham). To ensure equal DNA loading, the DNA concentration in each extract was determined fluorimetrically using PicoGreen (Molecular Probes/Invitrogen). Covalent TOP1–DNA complexes were then detected by immunoblotting with anti-TOP1 polyclonal anti- bodies (sc-32736, Santa Cruz.) and visualised by chemiluminescence.

Neutral single-cell agarose gel electrophoresis (Comet) assays

HEK293 cells at density (60,000 cell/24well plates) were seeded at 37°C overnight. In the second day cells were transfected using polyethyleneimine (PEI) 1μg/μl transfection reagent with plasmid DNA 500 ng/well. Transfected cells were incubated at 37°C for 24h then the complete media replaced with 1% FBS media and incubated for an additional 48h. Transfection efficiency was assessed at ~75%. Cells were suspended in pre-chilled phosphate buffered saline (PBS) and mixed with equal volume of low-gelling-temperature agarose 1.3% (Sigma, Type VII) preserved at 42°C. Cell mixture was immediately spread onto pre-chilled frosted glass slides (Fisher), pre-coated with 0.6% agarose. The slides were incubated at 4°C in the dark until set, and for all further steps. Slides were incubated in pre-chilled lysis buffer (2.5 M NaCl, 10 mMTris-base, 100mM EDTA (pH 8.0), 0.5% Triton X-100, 1% N-laurylsarcosine sodium salt and 3% DMSO; pH9.5) for 2 h. After incubation time slides washed with pre-chilled distilled H2o (2-10 min), and immersed for 1h in pre-chilled electrophoresis buffer (300mM sodium acetate, 100mM Tris-HCl, 1% DMSO, pH8.3). Then electrophoresis was conducted for 60 min at 1 V/cm, accompanied by washing 3 times with neutralization in 400 mM Tris- HCl (pH 7.5) for 15min. Finally, slides was stained with DNA Sybr Green I nucleic (1:10000, in PBS) (Sigma) for 30 min. Tail moments average from 100 cells per sample were counted using Comet Assay IV software (Perceptive Instruments, UK).

Generation of AAV9-mediated mice

3×10^{10} vg of purified scAAV was injected into the cisterna magna of C57BL/6J P1 wild-type mice under general anaesthesia. Postnatal day 1 (P1) Pups were placed over a red light

torch in prone position to enable visualisation of the injection site. scAAV was loaded into a 5ul syringe and the virus were injected under a flow rate of 1μl/min. Animals were housed in groups of up to 5 per cage. Gender splits for each group was as followed: 0-V5 (6M and 6F), 69-V5 (7M and 6F), 10-RRE (2M and 1F) and 102-RRE (2M and 1F). Six or 12 months after injection, mice were sacrificed under terminal anaesthesia and transcardially perfused using a solution of PBS-Heparin. Brain sections were then isolated and fixed using 4% PFA overnight at 4°C. After fixation, tissue was washed with PBS, cryoprotected in 30% of sucrose at 4°C and embedded in OCT (Cell Path®). 20 or 40μm brain coronal sections were derived using a cryostat, and then analysed using immunohistochemistry. Alternatively, brainstem portions were snap frozen in liquid nitrogen and were then lysed in RIPA buffer for Western Blotting analysis. All animal *in vivo* experiments were approved by the University of Sheffield Ethical Review Committee and performed according to the Animal (Scientific Procedures) Act 1986, under the Project License 40/3739. Animals were administered with AAV9 vectors at postnatal day 1 (P1). To mitigate potential confounding of treatment with litter effects a randomised block allocation design was used to ensure animals from a given litter were stratified across different treatment arms. Where there is only a single viable P1 pup in the litter, this was not allocated to treatment.

Whole animal neurological assays

All our behavioural testing was performed the same time of day (10.00 12.00). Gait and locomotion analysis at 6 months was performed by using the Catwalk system version 7.1. Briefly, 6 month old mice (n=12, 13 for 0-V5, 69-V5; respectively) were placed on the Catwalk machine and crossed a glass plate in darkness whilst footprints were captured and recorded using the Catwalk 7.1 software. Each animal performed the Catwalk assay up to six times and the best three runs were selected for analysis. Gait parameters (stand time, swing speed and stride length) were calculated for each limb using the Catwalk 7.1 software. Power analysis using GPower version 3.0.3 was used to determine sample sizes. Based on α of 0.05 and a power of 80% (β=0.8) a sample size of 12 is required to detect a decrease in Catwalk performance of 20% at 6 months of age. Neuroscoring analysis was performed in mice aged 12 months (0-V5, n=8; 69-V5, n=9). Briefly, mice were suspended by the tail and the splay defects were observed and scored individually for right and left hind-limbs, using a scale described previously: 0 normal splay; 1; mild defect; 2: moderate defect; 3: strong splay defect; 4 paralysed53. All behavioural tests were performed in blinded conditions, though neuroscoring splay analysis was performed under double-blinded conditions by a single observer.

Image Acquisition and Analysis

All representative images presented are Z stack projections acquired on a Leica SP5 confocal microscope, using the 63x 1.20 lens. For imaging cell monolayers, each stack was performed at 0.5μm intervals, scanning the entire nucleus. In tissue sections images were acquired using 1μm Z stacks. Fluorescence intensity quantification was performed according to a method described previously54 with some modifications. Using Image J, the corrected nuclear fluorescence value of the relevant channel was calculated using the formula: *Corrected Nuclear Fluorescence (CNF) = Integrated Nuclear Density (IND) – Nuclear Area (NA) x Mean Fluorescence of Background (MFB).* For *in vitro* foci counting, quantification

Europe PMC Funders Author Manuscripts

was performed under the 100x lens of a Nikon Eclipse Ni microscope, with 20-100 cells/condition assessed (as indicated in the respective figure legend). For quantification of mice brain sections, brainstem or cerebellar sections were imaged on a confocal microscope, as described above, and analysed manually, with one exception: For γH2AX analysis in mice expressing 0, 69 DPRs, foci quantification was automated, using image J. For human spinal cord sections, images were acquired using a Nikon Eclipse N*i* microscope under the 100x and 20x objective lenses. Large motor neurons located in the ventral horn of spinal cord sections were considered for analysis, ~50 motor neurons (minimum 25) were analysed from 6 *C9orf72*-ALS samples and 6 non-ALS samples. Motor neurons were considered R-Loop or γH2AX positive when the whole nucleus was stained positive. We employed a double-blind randomization process in which experimental groups and the protein being analysed were blinded to the person analysing the data (e.g. counting nuclear foci or taking micrographs). For H3K9me3 analysis, 4 controls and 4 *C9orf72*-ALS were imaged using a Leica LP5 confocal microscope and the mean fluorescence intensity (minus background signal) was calculated from 20 motor neurons per case.

Experimental repeats and Statistical analysis

All data are presented as the means ± standard errors of the mean (SEM) of 3 biological replicates, unless otherwise stated. Statistical differences were analysed using Student's t-tests for pair-wise comparisons or one-way ANOVA (with Tukey's correction) for comparing groups more than 2 but less than 9. A p-value less than 0.05 was considered to be statistically significant. Asterisks denote p values <0.05, double-asterisks denote p values <0.01, and triple asterisks denote p values <0.001, NS denotes p values >0.05.

Supplementary Material

Refer to Web version on PubMed Central for supplementary material.

Acknowledgements

M.A. and S.F.E-K made equal financial contribution to the work through the European Research Council Award (294745) and the Wellcome Trust Investigator Award (103844), respectively. S.F.E-K is funded by a Wellcome Trust Investigator Award (103844), a Lister Institute of Preventative Medicine Fellowship, and a European Union British Council award. M.A. is funded by the European Research Council (ERC Advanced Award no. 294745) and MRC DPFS Award (129016/G1001492). C.L., S-C.C., M.J., S.R. and C.W. (50%), were supported by the Wellcome Trust Investigator Award (103844). E.K. was supported by Eve Davis Studentship. S.H.M., I.T, V.L., K.L., J.C. and C.W. (50%) were supported by the ERC Advanced Award (294745). P.J.S and G.M.H are supported by the Medical Research Council (MR/M010864/1) and P.J.S is supported as an NIHR Senior Investigator. K.D.V is supported by the Thierry Latran Foundation (Project RoCIP) and Medical Research Council (MR/K005146/1 and MR/M013251/1). We thank Adrian Isaacs for providing the original DPR plasmids, Grant Stewart for providing the RNF168 plasmid and Lynne Baxter for the immunohistochemistry of post-mortem sections.

References

1. Schottlaender LV, et al. Analysis of C9orf72 repeat expansions in a large series of clinically and pathologically diagnosed cases with atypical parkinsonism. Neurobiol Aging. 2015; 36:1221.e1–6.
2. Rutherford NJ, et al. Length of normal alleles of C9ORF72 GGGGCC repeat do not influence disease phenotype. Neurobiol Aging. 2012; 33:2950.e5–7.
3. DeJesus-Hernandez M, et al. Expanded GGGGCC hexanucleotide repeat in noncoding region of C9ORF72 causes chromosome 9p-linked FTD and ALS. Neuron. 2011; 72:245–256. [PubMed: 21944778]

4. Groh M, Gromak N. Out of Balance: R-loops in Human Disease. PLoS Genet. 2014; 10:e1004630. [PubMed: 25233079]
5. Roy D, Yu K, Lieber MR. Mechanism of R-loop formation at immunoglobulin class switch sequences. Mol Cell Biol. 2008; 28:50–60. [PubMed: 17954560]
6. Aguilera A, García-Muse T. R Loops: From Transcription Byproducts to Threats to Genome Stability. Molecular Cell. 2012; 46:115–124. [PubMed: 22541554]
7. Haeusler AR, et al. C9orf72 nucleotide repeat structures initiate molecular cascades of disease. Nature. 2014; 507:195–200. [PubMed: 24598541]
8. Bhatia V, et al. BRCA2 prevents R-loop accumulation and associates with TREX-2 mRNA export factor PCID2. Nature. 2014; 511(7509):362–5. [PubMed: 24896180]
9. Yuce-Petronczki O, West SC. Senataxin, defective in the neurogenerative disorder AOA-2, lies at the interface of transcription and the DNA damage response. Mol Cell Biol. 2012; 33(2):406–17. [PubMed: 23149945]
10. Lindquist SG, et al. Corticobasal and ataxia syndromes widen the spectrum of C9ORF72 hexanucleotide expansion disease. Clin Genet. 2013; 83:279–283. [PubMed: 22650353]
11. Corcia P, et al. Pure cerebellar ataxia linked to large C9orf72 repeat expansion. Amyotroph Lateral Scler Frontotemporal Degener. 2016; 17(3–4):301–3. [PubMed: 26609732]
12. McKinnon PJ. ATM and the molecular pathogenesis of ataxia telangiectasia. Annu Rev Pathol Mech Dis. 2012; 7:303–321.
13. Shiloh Y, Ziv Y. The ATM protein kinase: regulating the cellular response to genotoxic stress, and more. Nature Reviews Molecular Cell Biology. 2013; 14:197–210.
14. Frappart P-O, et al. An essential function for NBS1 in the prevention of ataxia and cerebellar defects. Nat Med. 2005; 11:538–544. [PubMed: 15821748]
15. Ashour ME, Atteya R, El-Khamisy SF. Topoisomerase-mediated chromosomal break repair: an emerging player in many games. Nat Rev Cancer. 2015; 15:137–151. [PubMed: 25693836]
16. Gómez-Herreros F, et al. TDP2 protects transcription from abortive topoisomerase activity and is required for normal neural function. Nat Genet. 2014; 46:516–521. [PubMed: 24658003]
17. Chiang S-C, et al. Mitochondrial protein-linked DNA breaks perturb mitochondrial gene transcription and trigger free radical–induced DNA damage. Science Advances. 2017; 3:e1602506–16. [PubMed: 28508041]
18. Harrigan JA, et al. Replication stress induces 53BP1-containing OPT domains in G1 cells. The Journal of Cell Biology. 2011; 193:97–108. [PubMed: 21444690]
19. Heo J-I, et al. ATM mediates interdependent activation of p53 and ERK through formation of a ternary complex with p-p53 and p-ERK in response to DNA damage. Mol Biol Rep. 2012; 39:8007–8014. [PubMed: 22576881]
20. Katyal S, et al. Aberrant topoisomerase-1 DNA lesions are pathogenic in neurodegenerative genome instability syndromes. Nat Neurosci. 2014; 17:813–821. [PubMed: 24793032]
21. Alagoz M, Chiang S-C, Sharma A, El-Khamisy SF. ATM deficiency results in accumulation of DNA-topoisomerase I covalent intermediates in neural cells. PLoS ONE. 2013; 8:e58239. [PubMed: 23626666]
22. Li J, et al. Nuclear accumulation of HDAC4 in ATM deficiency promotes neurodegeneration in ataxia telangiectasia. Nat Med. 2012; 18:783–790. [PubMed: 22466704]
23. Zhang Y-J, et al. C9ORF72 poly(GA) aggregates sequester and impair HR23 and nucleocytoplasmic transport proteins. Nat Neurosci. 2016; 19:668–677. [PubMed: 26998601]
24. Difilippantonio S, et al. Role of Nbs1 in the activation of the Atm kinase revealed in humanized mouse models. Nat Cell Biol. 2005; 7:675–685. [PubMed: 15965469]
25. Schwertman P, Bekker-Jensen S, Mailand N. Regulation of DNA double-strand break repair by ubiquitin and ubiquitin-like modifiers. Nature Reviews Molecular Cell Biology. 2016; 17:379–394. [PubMed: 27211488]
26. Shanbhag NM, Rafalska-Metcalf IU, Balane-Bolivar C, Janicki SM, Greenberg RA. ATM-dependent chromatin changes silence transcription in cis to DNA double-strand breaks. Cell. 2010; 141:970–981. [PubMed: 20550933]

27. Bohgaki M, et al. RNF168 ubiquitylates 53BP1 and controls its response to DNA double-strand breaks. Proc Natl Acad Sci USA. 2013; 110:20982–20987. [PubMed: 24324146]
28. Fradet-Turcotte A, et al. 53BP1 is a reader of the DNA-damage-induced H2A Lys 15 ubiquitin mark. Nature. 2013; 499:50–54. [PubMed: 23760478]
29. Doil C, et al. RNF168 binds and amplifies ubiquitin conjugates on damaged chromosomes to allow accumulation of repair proteins. Cell. 2009; 136:435–446. [PubMed: 19203579]
30. Noon AT, et al. 53BP1-dependent robust localized KAP-1 phosphorylation is essential for heterochromatic DNA double-strand break repair. Nat Cell Biol. 2010; 12:177–184. [PubMed: 20081839]
31. Lee J-H, Goodarzi AA, Jeggo PA, Paull TT. 53BP1 promotes ATM activity through direct interactions with the MRN complex. EMBO J. 2010; 29:574–585. [PubMed: 20010693]
32. Stewart G, et al. The RIDDLE syndrome protein mediates a ubiquitin-dependent signaling cascade at sites of DNA damage. Cell. 2009; 136(3):420–34. [PubMed: 19203578]
33. Wang Y, et al. Autophagy Regulates Chromatin Ubiquitination in DNA Damage Response through Elimination of SQSTM1/p62. Molecular Cell. 2016; 63:34–48. [PubMed: 27345151]
34. Mann DMA, et al. Dipeptide repeat proteins are present in the p62 positive inclusions in patients with frontotemporal lobar degeneration and motor neurone disease associated with expansions in C9ORF72. Acta Neuropathol Commun. 2013; 1:68. [PubMed: 24252525]
35. Davidson YS, et al. Brain distribution of dipeptide repeat proteins in frontotemporal lobar degeneration and motor neurone disease associated with expansions in C9ORF72. Acta Neuropathol Commun. 2014; 2:70. [PubMed: 24950788]
36. Tresini M, Marteijn JA, Vermeulen W. Bidirectional coupling of splicing and ATM signaling in response to transcription-blocking DNA damage. rnabiology. 2017; 13:1–8.
37. Tresini M, et al. The core spliceosome as target and effector of non-canonical ATM signalling. Nature. 2015; 523(7558):53–8. [PubMed: 26106861]
38. Bakkenist CJ, Kastan MB. DNA damage activates ATM through intermolecular autophosphorylation and dimer dissociation. Nature. 2003; 421:499–506. [PubMed: 12556884]
39. Belzil VV, et al. Reduced C9orf72 gene expression in c9FTD/ALS is caused by histone trimethylation, an epigenetic event detectable in blood. Acta Neuropathol. 2013; 126:895–905. [PubMed: 24166615]
40. Goodarzi AA, et al. ATM signaling facilitates repair of DNA double-strand breaks associated with heterochromatin. Mol Cell. 2008; 31:167–177. [PubMed: 18657500]
41. Meisenberg C, et al. Epigenetic changes in histone acetylation underpin resistance to the topoisomerase I inhibitor irinotecan. Nucleic Acids Res. 2017; 45(3):1159–1176. [PubMed: 28180300]
42. Felisbino MB, Gatti MSV, Mello MLS. Changes in chromatin structure in NIH 3T3 cells induced by valproic acid and trichostatin A. J Cell Biochem. 2014; 115:1937–1947. [PubMed: 24913611]
43. Sanz LA, et al. Prevalent, dynamic, and conserved R-Loop structures associate with specific epigenomic signatures in mammal. Molecular Cell. 2016; 63(1):167–78. [PubMed: 27373332]
44. Castellano-Pozo M, et al. R loops are linked to histone H3 S10 phosphorylation and chromatin condensation. Molecular Cell. 2013; 52:583–590. [PubMed: 24211264]
45. Zhang Y, et al. Attenuated DNA damage repair by trichostatin A through BRCA1 suppression. Radiat Res. 2007; 168:115–124. [PubMed: 17722998]
46. Wang X, et al. Alzheimer disease and amyotrophic lateral sclerosis: an etiopathogenic connection. Acta Neuropathol. 2014; 127:243–256. [PubMed: 24136402]
47. El-Khamisy SF, et al. Defective DNA single-strand break repair in spinocerebellar ataxia with axonal neuropathy-1. Nature. 2005; 434:108–113. [PubMed: 15744309]
48. El-Khamisy SF. To live or to die: a matter of processing damaged DNA termini in neurons. EMBO Mol Med. 2011; 3:78–88. [PubMed: 21246735]
49. Chan YA, et al. Genome-wide profiling of yeast DNA:RNA hybrid prone sites with DRIP-chip. PLoS Genet. 2014; 10:e1004288. [PubMed: 24743342]
50. Zu T, et al. RAN proteins and RNA foci from antisense transcripts in C9ORF72 ALS and frontotemporal dementia. Proc Natl Acad Sci USA. 2013; 110:E4968–77. [PubMed: 24248382]

51. McIntyre GJ, Groneman JL, Tran A, Applegate TL. An infinitely expandable cloning strategy plus repeat-proof PCR for working with multiple shRNA. PLoS ONE. 2008; 3:e3827. [PubMed: 19043584]

52. Cooper-Knock J, et al. Sequestration of multiple RNA recognition motif-containing proteins by C9orf72 repeat expansions. Brain. 2014; 137:2040–2051. [PubMed: 24866055]

53. Mead RJ, et al. Optimised and rapid pre-clinical screening in the SOD1(G93A) transgenic mouse model of amyotrophic lateral sclerosis (ALS). PLoS ONE. 2011; 6:e23244. [PubMed: 21876739]

54. McCloy RA, et al. Partial inhibition of Cdk1 in G 2 phase overrides the SAC and decouples mitotic events. Cell Cycle. 2014; 13:1400–1412. [PubMed: 24626186]

Europe PMC Funders Author Manuscripts

Europe PMC Funders Author Manuscripts

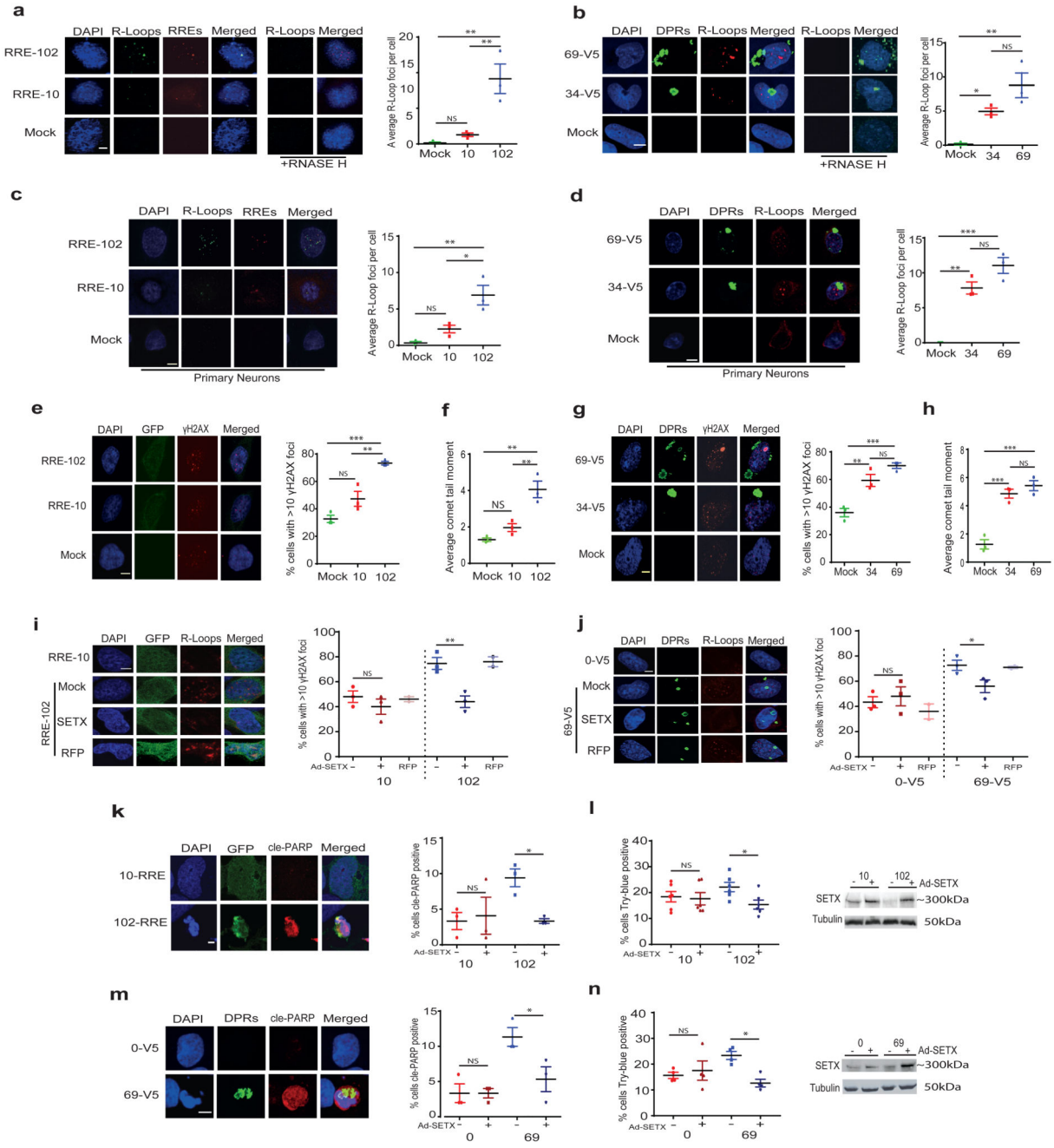

Figure 1. Expression of C9orf72 expansions leads to R-loop-driven DSBs and cellular toxicity.

(a) MRC5 cells mock transfected or transfected with 10 or 102 RREs. FISH-IF was performed using a G4C2 fluorescent probe ‘RNA’ and S9.6 antibodies ‘R-Loops’. Cells were treated with RNase H1 ‘+RNASE H’. *Left,* Representative images shown, scale bar 5 μm. *Right*, The average (± SEM) number of nuclear S9.6 foci per cell was quantified from 3 cell culture replicates, 50 cells each. Significance assessed using a one-way ANOVA. **(b)** MRC5 cells mock transfected or transfected with 34 or 69 poly-GA DPRs. Cells examined by immunocytochemistry using anti-V5 ‘DPRs’ and S9.6 antibodies ‘R-Loops’. *Left,*

Representative images are shown, scale bar 5μm. *Right,* S9.6 foci was quantified, presented, and analysed as described for (a). **(c,d)** Rat cortical neurons transduced with AAV9 viral-vectors encoding 10,102 RREs (c) or 34, 69 DPRs (d) were processed with FISH-IF double staining (c) or with immunocytochemistry (d), as described for (a,b). *Left,* Representative images shown, scale bar 5μm. *Right*, S9.6 foci quantified from 3 seperate neuronal preperations, 20 neurons each, and data presented and analysed as described for (a). **(e,g)** MRC5 cells mock transfected or were transfected with 10,102 RREs (with GFP) (e) or 34, 69 DPRs (g). Cells were immunostained with anti-γH2AX antibodies 'γH2AX', with GFP (e) or anti-V5 antibodies 'DPRs' (g). *Left,* Representative images are shown, scale bar 5μm. *Right,* The percentage of cells with 10 or more foci was quantified, presented and analysed as described for (a). **(f,h)** HEK 293T cells mock transfected, transfected with 10,102 RREs (f), or 34, 69 DPRs (h). Neutral comet tail moments were quantified, 100 cells each, presented, and analysed as described for (a).**(i-j)** MRC5 cells mock transduced or transduced with adenoviral vectors encoding for SETX or RFP and then transfected with 10 or 102 RREs (with GFP) (i) or with 0, 69 DPRs (j). *Left,* Cells were immunostained with S9.6 antibodies 'R-Loops' alongside GFP (i) or alongside anti-V5 'DPRs' antibodies (j). Representative images are shown, scale bar 5μm. *Right,* Cells were immunostained with anti-γH2AX antibodies as described for panels (e,f), and the average (± SEM) percentage of cells exhibiting 10 or more γH2AX foci was quantified, 25 cells each, and analysed using Student's t-test. **(k,m)** MRC5 cells transduced with adenoviral vector particles encoding for SETX or mock transduced and transfected with constructs encoding 10, 102 RREs (k) or 0 or 69 DPRs (m). Cells examined by immunocytochemistry using cleaved-PARP (Cell Signalling, 9548) 'cle-PARP' antibodies alongside GFP (k) or anti-V5 (Bethyl, A190-120A) 'DPRs' antibodies (m). *Left,* Representative images of cle-PARP-postive and -negative cells shown, scale bar 5μm. *Right,* the percentage of cells cleaved-PARP-positive was quantified, 50-100 cells each, presented and analysed as decribed for (i,j). **(l,n)** HEK 293T cells were mock transduced or transduced with adenoviral vector particles encoding for SETX and transfected with 10,102 RREs (l) or 0 or 69 DPRs (n). *Left,* Cells were analysed using Trypan blue exlusion assays, and the % of cells Trypan-permeable was quantified from 6 (l) and 4 (n) cell culture replicates, ~200 cells each, and was presented and analysed as decribed for (i,j). *Right*, Whole cell lysates from samples used in (l) and (n) were analysed by western blotting, using senataxin and anti-α-tubulin antibodies.

Europe PMC Funders Author Manuscripts

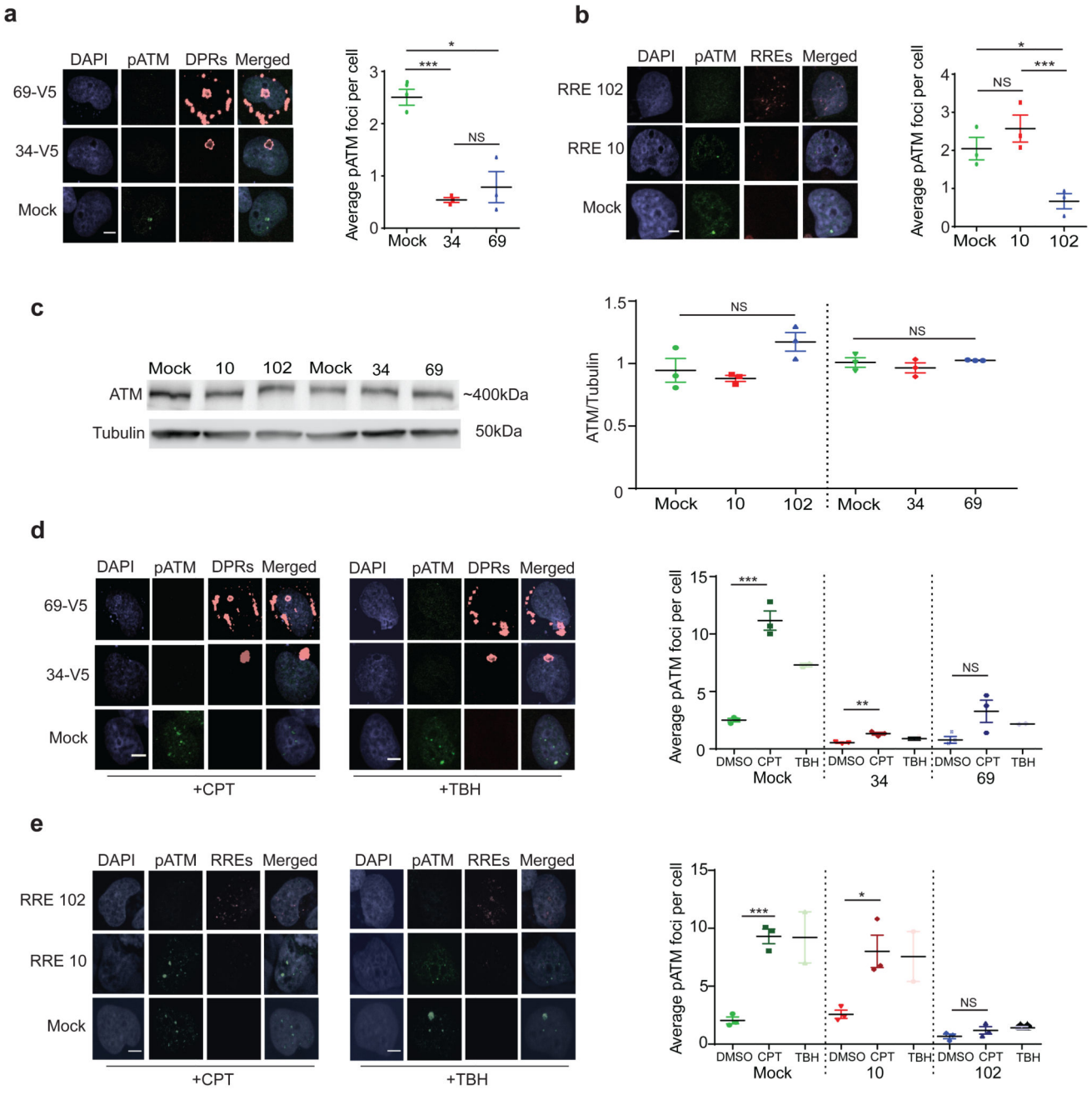

Figure 2. Expression of C9orf72 expansions leads to defective ATM activation.

(a,b) MRC5 cells mock transfected, transfected with 34, 69 DPRs (a), or 10, 102 RREs (b). Cells analysed using immunocytochemistry with anti-phosphorylated ATM 'pATM' and anti-V5 'DPRs' antibodies (a) or with FISH-IF (b). *Left,* Representative images shown, scale bar 5μm. *Right*, The average (± SEM) number of pATM foci per cell was quantified from 3 cell culture replicates, 50 cells each, and analysed using a one-way ANOVA. **(c)** *Left*, HEK 293T cells were mock transfected 'M' or were transfected constructs encoding 10 or 102 RREs '10, 102' or 34, 69 DPRs '34, 69'. Whole cell lysates were analysed using anti-ATM

and α-tubulin antibodies. *Right*, ATM protein expression (normalised to α-tubulin) is presented as average ± SEM from 3 cell culture replicates, and analysed using a one-way ANOVA. **(d,e)** MRC5 cells mock transfected, transfected with constructs encoding 34, 69 DPRs (d), or transfected with constructs encoding for 10, 102 RREs (e). Cells were incubated with 10μM CPT ,0.037% TBH, or DMSO for 1 hour, and analysed by immunocytochemistry as decribed for (a,b). *Left*, Representative images of 3 cell culture replicates are shown, scale bar 5μm. *Right*, pATM foci were quantified as decribed for (a,b).

Europe PMC Funders Author Manuscripts

Europe PMC Funders Author Manuscripts

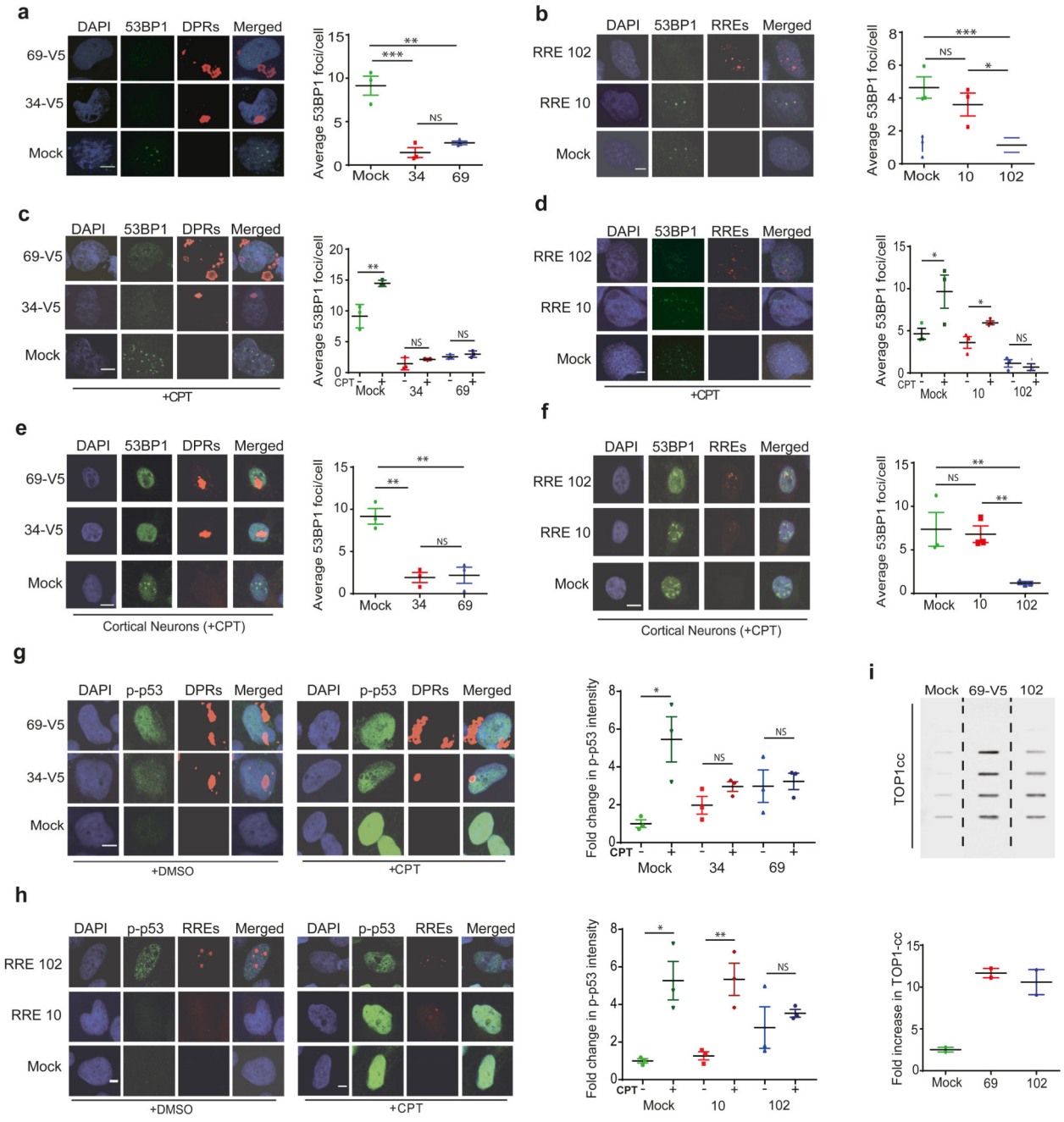

Figure 3. Expression of C9orf72 expansions leads to defective ATM signalling.

(a,b) MRC5 cells mock transfected or transfected with 34 or 69 DPRs (a) or 10, 102 RREs (b), and immunostained with anti-53BP1 antibodies, alongside anti-V5 'DPRs' antibodies or with FISH-IF double-staining 'RNA' (b). *Left*, Representative images are shown, scale bar 5μm. *Right*, The average (± SEM) number of 53BP1 foci per cell was quantified from 3 cell culture replicates, 50 cells each, and analysed using a one-way ANOVA. **(c,d)** MRC5 cells were mock transfected or transfected with constructs encoding 34 or 69 DPRs (c), or 10, 102 RREs (d). Cells were incubated with 10μM CPT or DMSO for 1hour, and immunostained as

described for (a,b). *Left,* Representative images are shown, scale bar 5μm. *Right*, 53BP1 foci was quantified as decribed above and analysed using a Student's t-test. **(e,f)** Rat cortical neurons mock transduced or transduced with AAV9 viral-vectors expressing 34 or 69 DPRs (e) or with 10 or 102 RREs (f). Neurons treated with 10μM CPT for 1 hour and analysed by immunocytochemistry as decribed for (a,b). *Left,* Representative images are shown, scale bar 5μm. *Right*, 53BP1 foci was quantified as decribed for (a,b), 20 neurons each, and analysed using a one-way ANOVA. **(g,h)** MRC5 cells were mock transfected or transfected with constructs encoding 34 or 69 DPRs (g), or 10, 102 RREs (h) and were then treated with DMSO or with 10μM CPT. Cells were then immunostained with anti-phosphorylated p53 antibodies, alongside anti-V5 'DPRs' antibodies (g) or with FISH-IF double-staining 'RNA' (h). *Left, R*epresentative images are shown, scale bar 5μm. *Right*, The nuclear fluorescence value for 50 nuclei was quantified from 3 cell culture replicates, and presented as the average (± SEM) fold change in nuclear intensity (relative to control cells), and analysed using Student's t-test. **(i)** *Top*, HEK 293T cells were mock transfected or were transfected with 69 DPRs or 102 RREs. Cells were treated 10μM CPT for 40 min, subjected to CsCl step gradients, and fractions slot blotted with anti-TOP1 antibodies. *Bottom*, The fold increase in TOP1-ccs, normalised to mock was calculated and presented as the average from 2 cell culture replicates ± range.

Europe PMC Funders Author Manuscripts

Europe PMC Funders Author Manuscripts

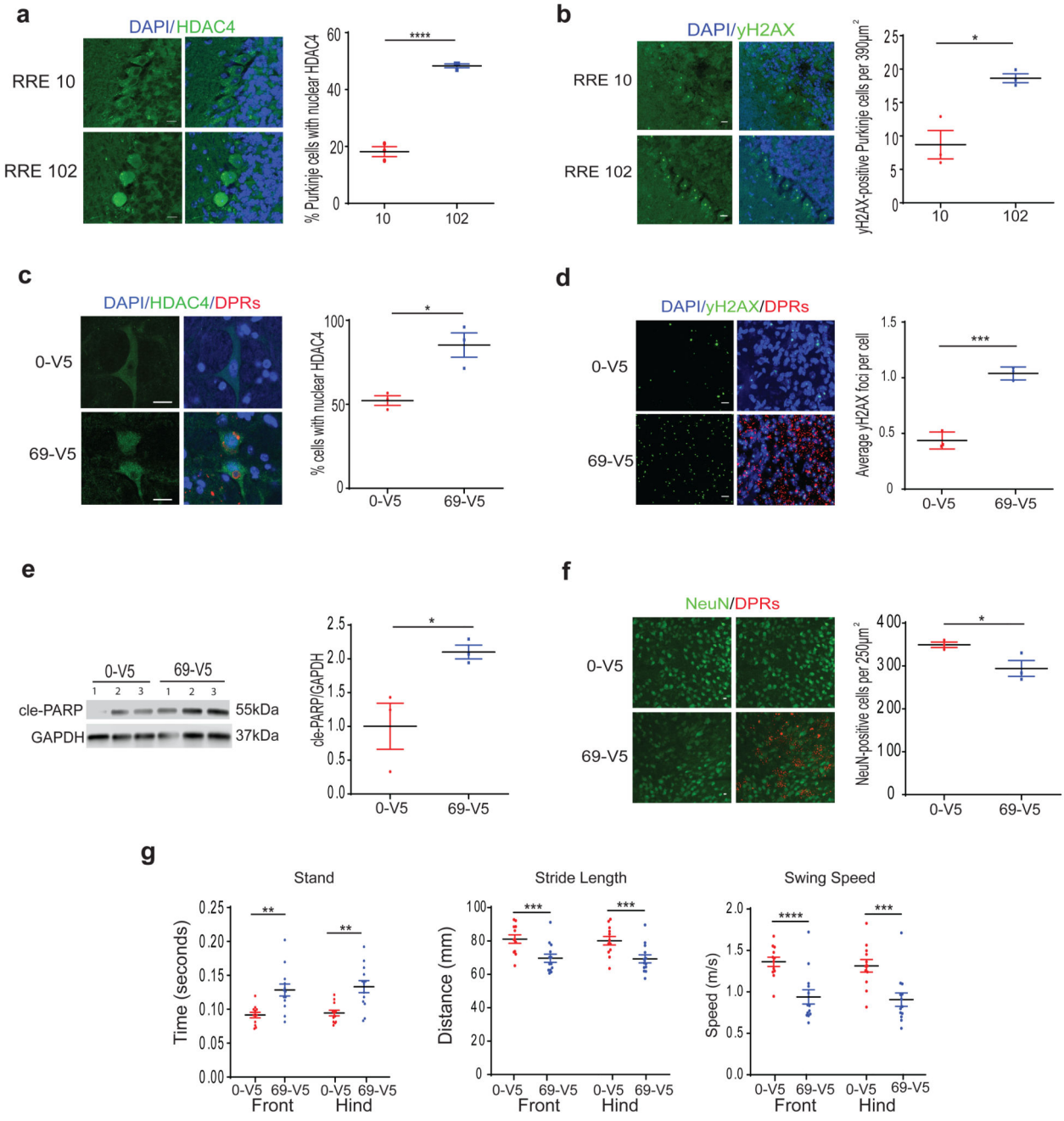

Figure 4. The expression of C9orf72 expansions in the murine CNS leads to DSBs, nuclear HDAC4, and neurodegeneration.

(a) Cerebellar sections from mice injected with AAV9-10 or -102 RREs subjected to immunohistochemistry using anti-HDAC4 antibodies. *Left,* Representative images shown, scale bar 10μm. *Right,* The average (± SEM) percentage of Purkinje cells displaying nuclear HDAC4 was calculated for 3 animals per group, 50 Purkinje cells per animal, and analysed using a Student's t-test. **(b)** Cerebellar sections from mice injected with AAV9-10 or -102 RREs subjected to immunohistochemistry using anti-γH2AX antibodies. *Left,*

*R*epresentative images shown, scale bar 10μm. *Right,* The average (± SEM) number of γH2AX-positive Purkinje cells was calculated from 3 animals per group, 10 images each, and analysed using a Student's t-test. **(c)** Brainstem sections from mice injected with AAV9-0 or -69 poly-GA DPRs were subjected to immunohistochemistry using anti-HDAC4 and anti-V5 antibodies. *Left, Re*presentative images shown, scale bar 10μm. *Right,* The average (± SEM) percentage of brainstem cells displaying nuclear HDAC4 was calculated for 3 animals per group, 30 HDAC4-positive cells per animal, and analysed using a Student's t-test. **(d)** Brainstem sections from mice injected with AAV9-0 or -69 poly-GA DPRs were subjected to immunohistochemistry using anti-γH2AX and anti-V5 antibodies. *Left, R*epresentative images shown, scale bar 10μm. *Right,* The average (± SEM) number of γH2AX foci per cell calculated from 3 animals per group, ~1000 cells per animal, and analysed using Student's t-test.**(e)** *Left,* Brainstem tissue harvested from mice injected with AAV9-0 or -69 poly-GA DPRs were analysed using Western blotting, with anti-GAPDH and anti-cleaved PARP antibodies. *Right,* cleaved-PARP was quantified and normalised to GAPDH, presented as the average intensity ± SEM from 3 animals per group, and analysed using a Student's t-test. **(f)** *Left,* Brainstem sections from mice injected with AAV9-0 or -69 poly-GA DPRs were subjected to immunohistochemistry using anti-NeuN and anti-V5 antibodies. The average (± SEM) number of NeuN-positive cells within the periaqueductal gray region of the brainstem was quantified from 3 animals per group, and analysed using Student's t-test. **(g)** Catwalk analysis was performed in animals injected with AAV9-0 or -69 poly-GA DPRs, aged 6 months. Stand intensity, stride length, and swing speed were quantified (n=12/13 for 0-V5/69-V5), presented as average ± SEM, analysed using Student's t-test.

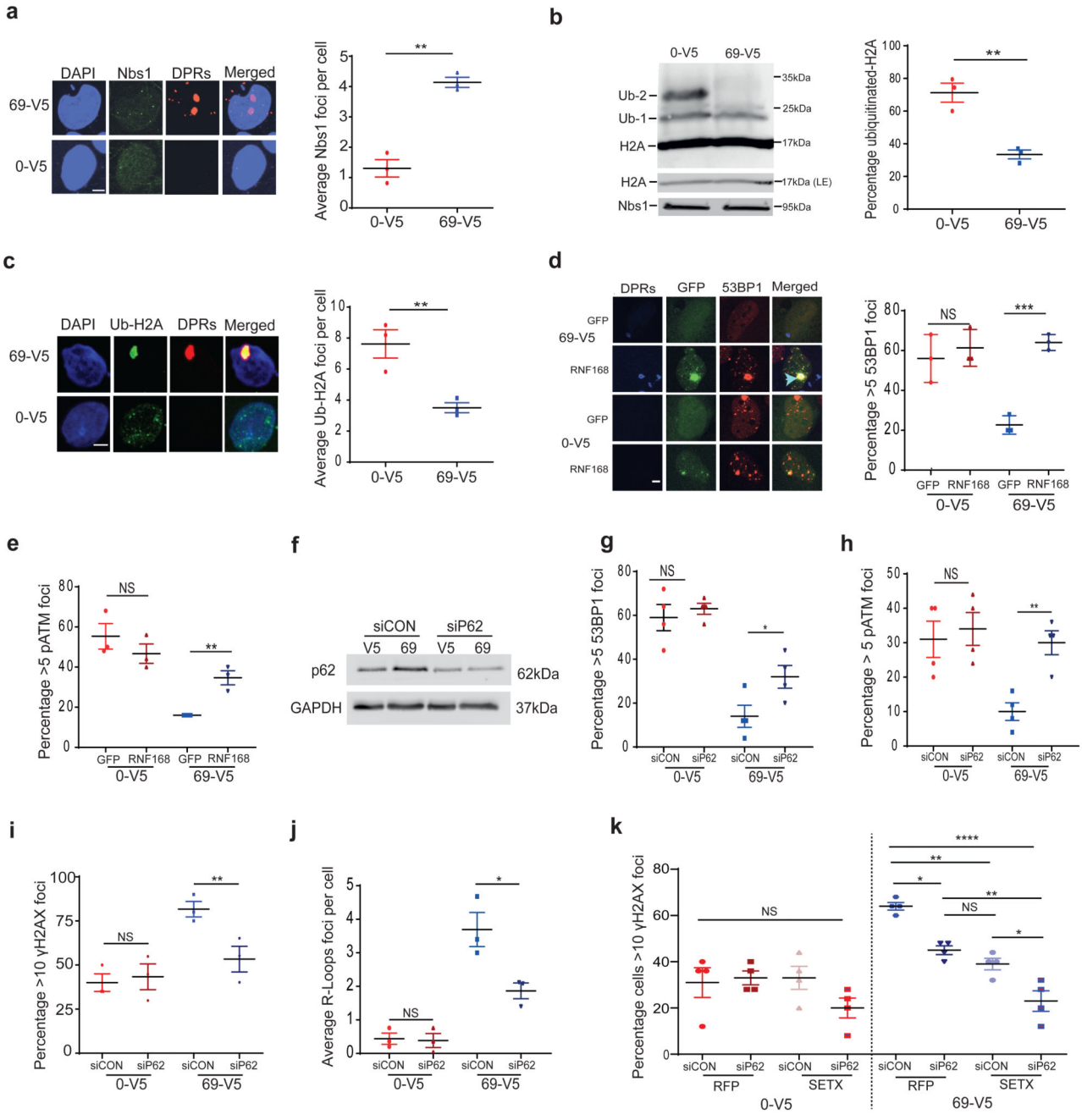

Figure 5. Defective ATM-mediated DNA repair can be restored by RNF168 overexpression or p62 depletion.

(a) MRC5 cells transfected with 0 or 69 DPRs, and immunostained with anti-V5 'DPRs' and anti-Nbs1 antibodies. *Left,* Representative images are shown, scale bar 5μm. *Right*, The average (± SEM) number of Nbs1 foci per cell was quantified and from 3 cell culture replicates, 50 cells each, and analysed using a Student's t-test. **(b)** *Left,* Chromatin fractions from MRC5 cells transfected with 0 or 69 DPRs were seperated analysed with Western blotting using antibodies specific to H2A . Low exposure (LE) H2A and Nbs1 bands show

equal loading. *Right,* The average (± SEM) percentage of H2A that was ubiqutinated was quantifed from 3 cell culture replicates and analysed using Student's t-test. **(c)** *Left,* MRC5 cells transfected with constructs encoding 0 or 69 DPRs, and immunostained with anti-V5 'DPRs' and anti-Ubiquinated-H2A 'Ub-H2A' antibodies. Representative images are shown, scale bar 5μm. *Right*, Ub-H2A foci was quantified, 25 cells each, presentaed and analysed as decribed for (a). **(d)** MRC5 cells transfected with constructs encoding 0 or 69 DPRs, and with control-GFP or RNF168-GFP, were immunostained with anti-V5 and anti-53BP1 antibodies. *Left*, Reprentative images are shown. *Right*, the percentage of cells with 5 or more 53BP1 foci was quantified (25 cells each), presented, and analysed as decribed for (a). **(e)** MRC5 cells transfected with constructs encoding 0 or 69 DPRs, and with control-GFP or RNF168-GFP plasmids, were immunostained with anti-V5 and anti-pATM antibodies. The percentage of cells with 5 or more pATM foci was quantified (25 cells each), presented and analysed as decribed for (a). **(f)** MRC5 cells transfected with constructs encoding 0 or 69 DPRs, with either control siRNA particles or p62 siRNA particles, were analysed with Western blotting using antibodies specific to p62 and GAPDH. **(g)** MRC5 cells transfected with constructs encoding 0 or 69 DPRs, and with control siRNA particles or p62 siRNA particles, were immunostained with anti-V5 and anti-53BP1 antibodies. The percentage of cells with 5 or more 53BP1 foci was quantified from 4 cell culture replications (25 cells each), presented and analysed as described for (a). **(h)** MRC5 cells transfected with constructs encoding 0 or 69 DPRs, and with control siRNA particles or p62 siRNA particles, were immunostained with anti-V5 and anti-pATM antibodies. The percentage of cells with 5 or more pATM foci was quantified from 4 cell culture replicates (25 cells each), presented and analysed as decribed for (a). **(i)** MRC5 cells transfected with constructs encoding 0 or 69 DPRs, with control siRNA particles or p62 siRNA particles. Cells were immunostained with anti-V5 'DPRs' and anti--γH2AX antibodies. The percentage of cells with 10 or more γH2AX foci was quantified (25 cells each), presented, and analysed as decribed for (a). **(j)** MRC5 cells transfected with constructs encoding 0 or 69 DPRs, with control siRNA particles or p62 siRNA particles, were immunostained with anti-V5 'DPRs' and anti—S9.6 antibodies. R-Loop foci were quantified, presented and analysed as described for (a).**(k)** MRC5 cells transduced with adenoviral vectors encoding for SETX or RFP, transfected with constructs encoding 0 or 69 DPRs, with control siRNA or p62 siRNA particles, were immunostained with anti-V5 and anti--γH2AX antibodies. Nuclei were counterstained with DAPI. The average (± SEM) percentage of cells with 10 or more γH2AX foci was quantified from 4 cell culture replicates (25 cells each), and analysed using a one-way ANOVA.

Europe PMC Funders Author Manuscripts

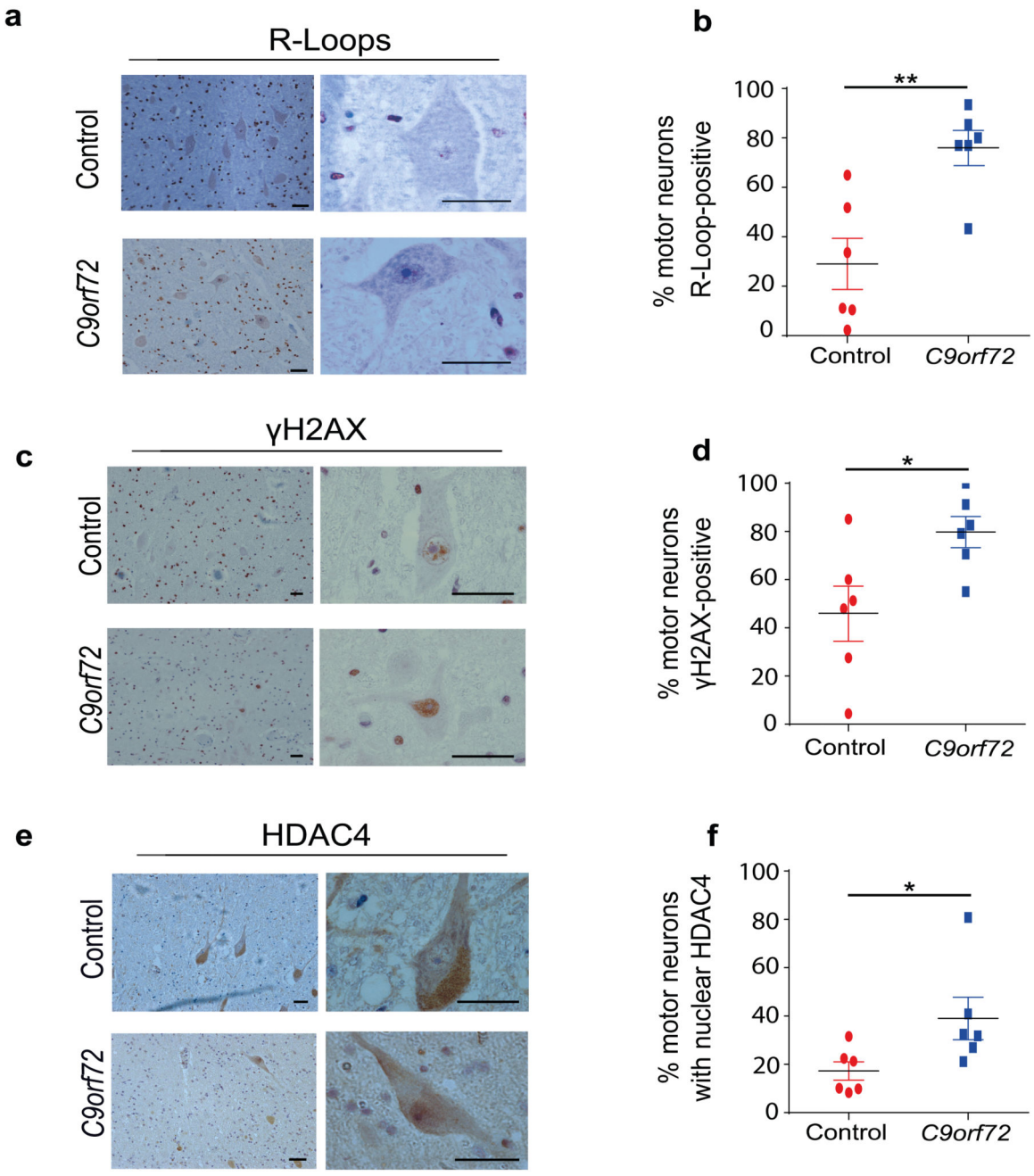

Figure 6. Spinal Cord Motor Neurons from *C9orf72*-ALS post-mortem show elevated levels of R-Loops, DSBs, and nuclear HDAC4.

(a) Human spinal cord sections were analysed by immunohistochemistry using S9.6 antibodies. Representative images are presented, scale bar 5μm. **(b)** The average (± SEM) percentage of R-Loop-positive motor neurons was quantified from 6 *C9orf72* patient and 6 control sections, ~50 cells each, and analysed with Student's t-test. **(c)** Human spinal cord sections were analysed by immunohistochemistry using anti-γH2AX antibodies. Representative images are presented, scale bar 5 μm. **(d)** The % of γH2AX-postive motor

neurons was quantified, presented and analysed as described for (b). **(e)** Human spinal cord sections were analysed by immunohistochemistry using anti-HDAC4 antibodies. Representative images are presented, scale bar 5 μm. **(f)** The % of motor neurons displaying HDAC4 enrichment in the nucleus was quantified, presented and analysed as described for (b).

Europe PMC Funders Author Manuscripts